iScience

CellPress
OPEN ACCESS

Article

Dorsal motor vagal neurons can elicit bradycardia and reduce anxiety-like behavior

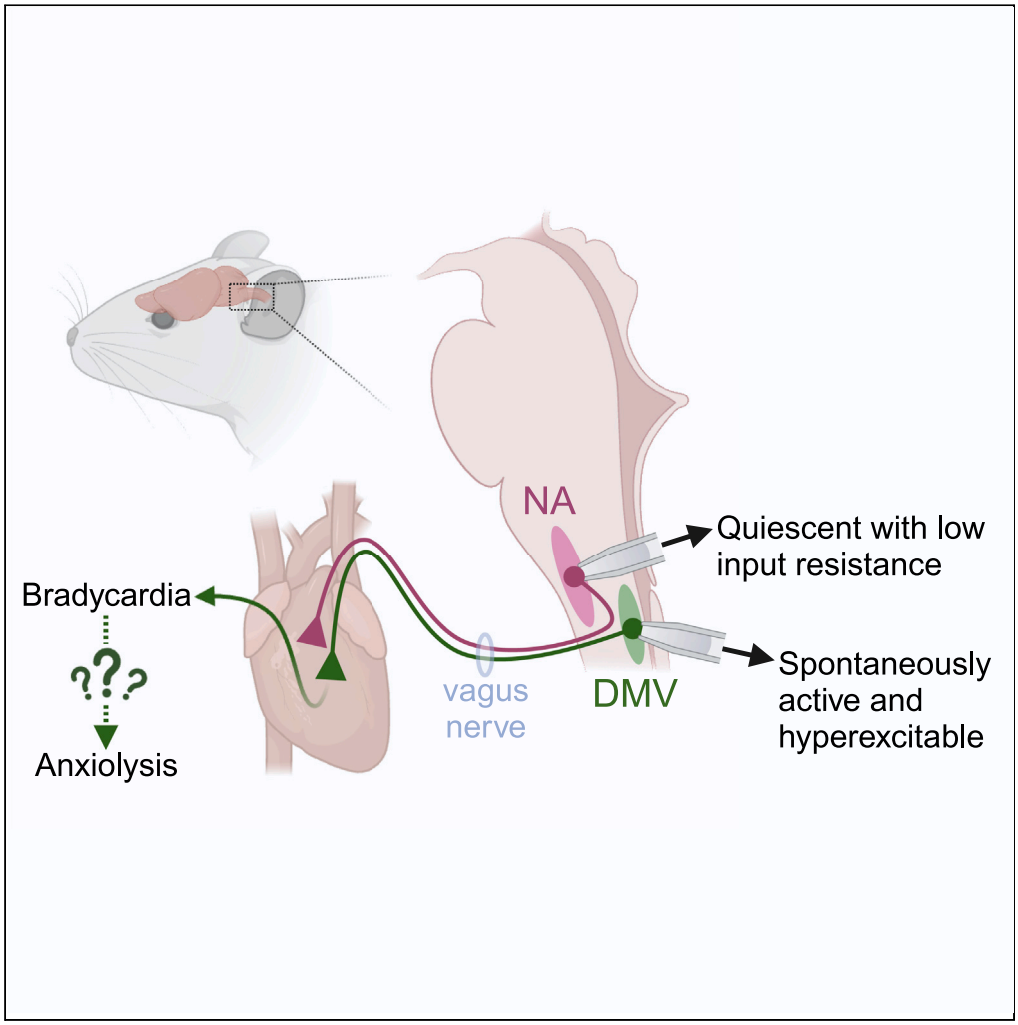

Misty M. Strain, Nicholas J. Conley, Lily S. Kauffman, ..., Ali D. Güler, John N. Campbell, Carie R. Boychuk

jnc4e@virginia.edu (J.N.C.)
boychukc@missouri.edu (C.R.B.)

Highlights

The brainstem's dorsal motor nucleus of the vagus contains cardiovagal neurons (DMV^{CVN})

DMV^{CVN} have unique electrophysiological properties compared to nucleus ambiguus

DMV^{CVN} can elicit bradycardia upon opto- or chemogenetic activation

DMV activity can reduce anxiety-related behavior

Strain et al., iScience *27*, 109137
March 15, 2024
https://doi.org/10.1016/j.isci.2024.109137

iScience

CellPress
OPEN ACCESS

Article

Dorsal motor vagal neurons can elicit bradycardia and reduce anxiety-like behavior

Misty M. Strain,[1,7] Nicholas J. Conley,[2,7] Lily S. Kauffman,[2,7] Liliana Espinoza,[1] Stephanie Fedorchak,[1] Patricia Castro Martinez,[3] Maisie E. Crook,[2] Maira Jalil,[2] Georgia E. Hodes,[4] Stephen B.G. Abbott,[5] Ali D. Güler,[2] John N. Campbell,[2,8,*] and Carie R. Boychuk[1,6,8,9,*]

SUMMARY

Cardiovagal neurons (CVNs) innervate cardiac ganglia through the vagus nerve to control cardiac function. Although the cardioinhibitory role of CVNs in nucleus ambiguus (CVN^{NA}) is well established, the nature and functionality of CVNs in dorsal motor nucleus of the vagus (CVN^{DMV}) is less clear. We therefore aimed to characterize CVN^{DMV} anatomically, physiologically, and functionally. Optogenetically activating cholinergic DMV neurons resulted in robust bradycardia through peripheral muscarinic (parasympathetic) and nicotinic (ganglionic) acetylcholine receptors, but not beta-1-adrenergic (sympathetic) receptors. Retrograde tracing from the cardiac fat pad labeled CVN^{NA} and CVN^{DMV} through the vagus nerve. Using whole-cell patch-clamp, CVN^{DMV} demonstrated greater hyperexcitability and spontaneous action potential firing *ex vivo* despite similar resting membrane potentials, compared to CVN^{NA}. Chemogenetically activating DMV also caused significant bradycardia with a correlated reduction in anxiety-like behavior. Thus, DMV contains uniquely hyperexcitable CVNs and is capable of cardioinhibition and robust anxiolysis.

INTRODUCTION

Cardiovagal neurons (CVNs) send axonal projections from hindbrain to cardiac ganglia through the vagus nerve to elicit cardioinhibitory (i.e., slowing of heart rate; HR) action at rest and during critical cardiorespiratory homeostatic reflexes. Although in mammals most CVNs are found in the nucleus ambiguus (CVN^{NA}), 20% of CVNs arise from a second region, the dorsal motor nucleus of the vagus (CVN^{DMV}).[1–6] While the ability of CVN^{NA} to control chronotropy (e.g., HR) is well characterized,[7–9] whether this ability extends to CVN^{DMV} remains controversial, despite their extensive innervation of cardiac tissue.[10] CVN^{DMV} innervate cardiac tissue with unmyelinated, C fibers,[11] the selective activation of which causes a bradycardia (or a decrease in HR) in multiple mammalian species.[12,13] In addition, studies of CVN ontogenesis implicate DMV, not NA, as the primary vagal nucleus in lower-order vertebrates and in early mammalian embryonic development, since CVN^{NA} migrate out of DMV,[14,15] making it possible that CVN^{DMV} retain functional cardioinhibitory activity in mammals.

Despite these anatomical studies, functional studies remain conflicting. Some argue that direct electrical stimulation of DMV does not change chronotropy,[7,16] while others demonstrate local activation (chemical, electrical, optogenetic, or chemogenetic) elicits bradycardias even if only modestly.[17–21] However, no activation technique in awake animals used to date rules out incidental stimulation of either neighboring nucleus tractus solitarius (NTS) neurons or inhibitory interneurons within DMV. Stimulation of this latter population could significantly dampen the impact of cholinergic premotor neuron stimulation. Thus, whether cholinergic CVN^{DMV} are capable of controlling chronotropy remains an important but open question.

A recent resurgence of interest in understanding of vagal physiology is driven by the growing number of therapeutic applications for vagus nerve stimulation.[22] Of particular interest, vagus nerve stimulation is a promising treatment for anxiety and post-traumatic stress disorder.[23,24] In rats, stimulating the vagus nerve accelerates extinction of conditioned fear[25,26] and decreases anxiety-like behavior in the elevated plus maze paradigm.[23] In humans, vagal nerve stimulation may even reduce treatment-resistant anxiety disorders.[27] However, the mechanism behind the anxiolytic effect of vagal stimulation is currently unknown. Since the vagus nerve is a bidirectional nerve, carrying sensory information from viscera to brain and motor information from brain to viscera, the extent to which the anxiolytic effect of vagus nerve stimulation

[1]Department of Cellular and Integrative Physiology, Long School of Medicine, University of Texas Health San Antonio, San Antonio, TX, USA
[2]Department of Biology, University of Virginia, Charlottesville, VA, USA
[3]Neuroscience Undergraduate Major, University of Virginia, Charlottesville, VA, USA
[4]School of Neuroscience, Virginia Polytechnic Institute and State University, Blacksburg, VA, USA
[5]Department of Pharmacology, University of Virginia, Charlottesville, VA, USA
[6]Dalton Cardiovascular Research Center, University of Missouri, Columbia, MO, USA
[7]These authors contributed equally
[8]Senior author
[9]Lead contact
*Correspondence: jnc4e@virginia.edu (J.N.C.), boychukc@missouri.edu (C.R.B.)
https://doi.org/10.1016/j.isci.2024.109137

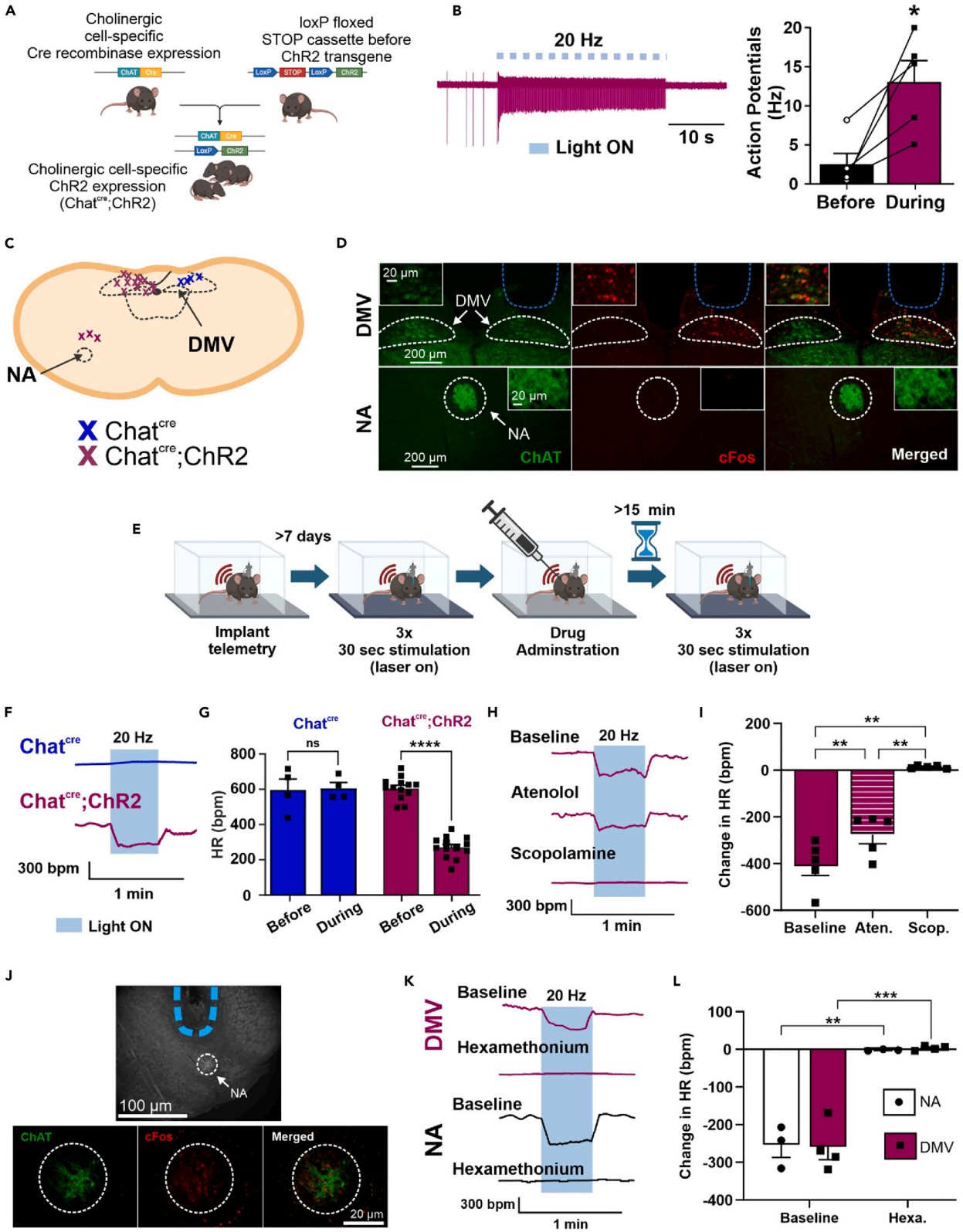
A
Cholinergic
cell-specific
Cre recombinase expression
loxP floxed
STOP cassette before
ChR2 transgene
Cholinergic cell-specific
ChR2 expression
(Chat^cre;ChR2)
B
20 Hz
Light ON
10 s
Action Potentials (Hz)
Before
During
C
DMV
NA
X Chat^cre
X Chat^cre;ChR2
D
DMV
NA
20 μm
200 μm
ChAT
cFos
Merged
E
>7 days
>15 min
Implant telemetry
3x 30 sec stimulation (laser on)
Drug Adminstration
3x 30 sec stimulation (laser on)
F
Chat^cre
Chat^cre;ChR2
20 Hz
300 bpm
1 min
Light ON
G
Chat^cre
Chat^cre;ChR2
ns
****
HR (bpm)
Before
During
H
Baseline
20 Hz
Atenolol
Scopolamine
300 bpm
1 min
I
Change in HR (bpm)
Baseline
Aten.
Scop.
J
NA
100 μm
ChAT
cFos
Merged
20 μm
K
DMV
NA
Baseline
20 Hz
Hexamethonium
300 bpm
1 min
L
Change in HR (bpm)
NA
DMV
Baseline
Hexa.

Figure 1. Optogenetic stimulation of DMV elicits bradycardia in male and female mice

Genetic crossbreeding paradigm used to generate transgenic mice harboring loxP-flanked ChR2 in Chat-positive motor neurons (A). Photostimulation-evoked action potentials from DMV motor neurons to 20 Hz stimulation (B). Representative diagram illustrating confirmed locations of optogenetic probes (C). Representative images of DMV (top) and NA (bottom) stained for the neuronal activation marker, c-Fos (middle panel; red) and GFP (left panel; green) immunoreactivity confirming c-Fos activation in DMV, but not NA, after DMV photostimulation (D). Schematic illustrating time course of optogenetic studies in awake mice (E). Representative trace (F) and mean HR (G) showing optogenetic stimulation of DMV produced a bradycardia in mice expressing $Chat^{cre}$;ChR2 but not in $Chat^{cre}$ mice. Representative trace (H) and mean HR (I) showing *i.p.* muscarinic parasympathetic blocker, methyl-scopolamine, eliminated the photostimulation-induced bradycardia, while sympathetic blockage with β-1 receptor blocker atenolol mildly reduced this bradycardia. Representative images of probe site (top) and immunohistochemical staining of NA showing c-Fos activation after stimulation of NA (J). Representative trace (K) and mean HR (L) showing the nicotinic antagonist, hexamethonium *(i.p.)* abolished photostimulation-induced bradycardia in both DMV and NA. Bars represent mean and SEM. Blue bars/shading indicates light stimulation. Data analyzed by a repeated measure one-way ANOVA with Tukey's post hoc (B and I) or repeated measure two-way ANOVA with Šídák's post hoc when appropriate (G and L). *$p \leq 0.05$, **$p \leq 0.01$, ***$p \leq 0.001$, ****$p \leq 0.0001$.

depends on sensory or motor signaling is unclear. One possibility is that activating the vagus nerve decreases anxiety by slowing HR, in line with the James-Lange theory of emotions.[28] Accordingly, a recent study in mice demonstrated that tachycardia (e.g., increase in HR) is sufficient to induce anxiety-like behavior.[29]

Controversy over the role of CVN^{DMV} may stem in part from differences in CVN^{NA} and CVN^{DMV} electrophysiology and thus their roles in regulating HR. Notably, CVN^{NA} are largely quiescent *in vivo* and *ex vivo*,[30,31] responding solely to integrated synaptic signaling. While limited data exist on the electrophysiological properties of CVN^{DMV} specifically, other DMV neuronal populations have unique pace-making properties and maintain a relatively high activity *ex vivo*,[32] which allows for more complex signal processing. One investigation into their activity also suggests that, unlike CVN^{NA}, CVN^{DMV} do not demonstrate robust respiratory burst patterning.[33] Therefore, it is tempting to speculate that CVN^{DMV} integrate and communicate central information differently from CVN^{NA} and represent a functionally unique circuit with respect to CVN^{NA}, which is consistent with evidence that CVN^{DMV} and CVN^{NA} target different cardiac ganglia.[34] A more extensive characterization of the electrophysiological properties of CVN^{DMV} will help build a foundation for understanding their cardioregulatory role, and importantly, for harnessing the therapeutic potential of vagus nerve stimulation. This is critical given that synaptic input to CVN^{DMV} is uniquely sensitive to perturbation of the cardiovascular system, relative to CVN^{NA}.[35]

The aim of the present study was to characterize the ability of DMV neurons to regulate HR functionally, physiologically, and pharmacologically. We hypothesized that activating choline acetyltransferase positive (Chat+) CVN^{DMV} elicits robust bradycardias. Moreover, we sought to characterize the electrophysiological properties of CVN^{DMV} to determine whether they are distinct from the more extensively studied CVN^{NA}. Testing of these hypotheses was accomplished using a combination of opto- and chemogenetic stimulation specifically in Chat+ neurons, pharmacological techniques to determine the regulatory role of CVN^{DMV} on chronotropy, and retrograde labeling paired with electrophysiology to examine differences between the two CVN populations. Our results raise the possibility that CVN^{DMV} play a role distinct from CVN^{NA} in regulating HR.

RESULTS

Optogenetic stimulation of Chat+ DMV can elicit bradycardia

To determine if CVN^{DMV} activation is capable of cardioinhibition, we used optogenetics to activate cholinergic neurons in DMV. Specifically, we crossed Ai32 mice expressing channelrhodopsin-2/EYFP fusion protein (ChR2) to *loxP* floxed choline acetyltransferase ($Chat^{cre}$) mice to selectively express ChR2 in Chat+ neurons ($Chat^{cre}$;ChR2). $Chat^{cre}$;ChR2 and $Chat^{cre}$ mice (Figure 1A) were implanted with HR telemetry devices and fiber optic probes above the right DMV. HR was examined before and during photostimulation. A preliminary study found that 20 Hz (−261 ± 32 bpm; n = 4 mice) elicited a significantly larger bradycardia compared to 5 (−58 ± 28 bpm; repeated measure one-way ANOVA with Šídák's post hoc, p = 0.0003), 10 (−126 ± 26 bpm; p = 0.0064), and 40 (−43 ± 16 bpm; p = 0.0002) Hz stimulation to DMV in $Chat^{cre}$;ChR2 mice (data not shown). We further verified that DMV neurons were continuously activated by 20 Hz photostimulation using whole-cell patch-clamp in brain slices from $Chat^{cre}$;ChR2 mice (before: 2.5 ± 1.4 Hz versus during: 13.0 ± 2.7 Hz; repeated measure one-way ANOVA with Tukey's post hoc, p = 0.0482; n = 5 neurons from two mice; Figure 1B). DMV neurons from $Chat^{cre}$;ChR2 mice also had lower firing frequencies immediately following stimulation (after: 1.4 ± 1.2 Hz; p = 0.0321), and they qualitatively demonstrated a pause immediately following stimulation termination that lasted for 10.3 ± 3.9 s with a range of 0.7–18 s.

Photostimulating DMV in awake male and female $Chat^{cre}$;ChR2 mice significantly affected HR compared to $Chat^{cre}$ mice. During photostimulation, $Chat^{cre}$;ChR2 decreased HR (271 ± 17 bpm) compared to HR before stimulation (605 ± 18 bpm; repeated measure two-way ANOVA with Šídák's post hoc, p < 0.0001; n = 13 mice; Figures 1F and 1G). Photostimulation failed to significantly affect HR during stimulation in control, $Chat^{cre}$ mice (before: 597 ± 61 bpm vs. during: 606 ± 31 bpm, p = 0.9633; n = 4 mice), confirming that photostimulation-induced bradycardia in $Chat^{cre}$;ChR2 was not a consequence of off-target effects or exposure to a laser (e.g., tissue necrosis, light diffusion, temperature effects). Finally, photostimulation-induced bradycardia in $Chat^{cre}$;ChR2 was significantly different from HR responses to light in $Chat^{cre}$ control (comparing both mouse lines during stimulation: p < 0.0001).

In contrast to photoexcitation of DMV neurons, photoinhibition of cholinergic neurons in DMV of awake mice using $Chat^{cre}$ mice crossed to Ai39 mice conditionally expressing halorhodopsin ($NpHR^{EYFP}$), produced no significant HR response to light (before: 629 ± 45 bpm vs. during: 627 ± 38 bpm; two-tailed paired Student's *t* test, p = 0.8950, n = 3 mice). While these results suggest that under these conditions DMV

neurons are sufficient to regulate HR but not necessary for control of resting HR, the decay kinetics of $NpHR^{EYFP}$ expressed by Ai39 mice are sufficiently fast enough that it might not cause a robust neural inhibition.[36]

Since the axons of CVN^{NA} travel dorsally to converge with axons from CVN^{DMV} before turning and exiting the brainstem (e.g.,[37]), it was possible that cardioinhibitory actions of DMV resulted from stimulating nearby CVN^{NA} axons. To rule out CVN^{NA} axonal stimulation, we first examined c-Fos expression in ChAT+ neurons 2 h post-DMV stimulation (Figure 1D). Qualitatively robust c-Fos was seen on the stimulated (right) side of DMV with no c-Fos expression in NA. We also confirmed using immunofluorescence that stimulating NA directly causes c-Fos expression (Figure 1J). Finally in a subset of anesthetized $Chat^{cre}$;ChR2 mice, photostimulation of the exposed vagus nerve produced no change in HR (before: 422 $\pm$ 61 bpm vs. during: 419 $\pm$ 60 bmp; two-tailed paired Student's *t* test, p = 0.9723; n = 3 mice). Taken together, axonal expression of ChR2 in NA was not sufficient to activate NA and elicit bradycardia.

DMV photostimulation-induced bradycardia works through canonical vagal circuits

To confirm that DMV photostimulation affects HR though autonomic pathways, male $Chat^{cre}$;ChR2 mice were administered an intraperitoneal (*i.p.*) injection of hexamethonium to block all nicotinic acetylcholine receptor (nAChR) communication between preganglionic and cardiac-projecting postganglionic parasympathetic neurons prior to DMV (n = 4) or NA (n = 3) photostimulation (Figure 1E). Photostimulating of DMV (−261 $\pm$ 32 bpm) decreased HR to a similar extent as photostimulating NA (−255 $\pm$ 32 bpm) (repeated measure two-way ANOVA, p = 0.8157). As expected, pretreatment with hexamethonium abolished photostimulation-induced bradycardias from both brainstem regions (HR responses in DMV: 3 $\pm$ 3 bpm and HR responses in NA: −2 $\pm$ 1, p < 0.0001; Figures 1J–1L), and HR was also not different between DMV and NA during photostimulation after pre-treatment with hexamethonium (p = 0.9931).

To confirm that muscarinic acetylcholine receptor (mAChR) signaling is necessary for DMV-induced bradycardia, $Chat^{cre}$;ChR2 mice received *i.p.* injections of scopolamine methylbromide (to block parasympathetic activity) and atenolol (to block sympathetic activity) in a randomized order prior to photostimulation (Figure 1E). In this subset of mice (n = 5), optogenetic activation of DMV neurons again induced robust bradycardia (−405 $\pm$ 46 bpm) (Figures 1H and 1I). Although administration of atenolol modestly reduced DMV light-induced bradycardias (−276 $\pm$ 39 bpm; repeated measure one-way ANOVA with Tukey's post hoc, p = 0.003; Figures 1H and 1I), atenolol also significantly decreased resting HR (before: 665 $\pm$ 21 vs. atenolol: 527 $\pm$ 10, p = 0.0093; n = 5). Using a simple linear regression, there was a significant negative relationship between resting HR and DMV light-induced bradycardia (R^2 = 0.4741, p = 0.0277). Therefore, it is likely that the impact of atenolol on DMV-related bradycardia is through overall reductions in resting HR, and not stimulation of postganglionic sympathetic pathways. Unlike atenolol, however, administering scopolamine methylbromide abolished DMV light-induced bradycardias (14 $\pm$ 3 bpm, p = 0.002, Figures 1H and 1I). Thus, both nAChR and mAChR activity is required for photostimulation-induced decreases in HR from DMV, similar to NA. Some reports suggest that DMV-mediated vagal activity on cardiac tissue occurs through non-canonical nAChR communication between postganglionic parasympathetic neurons to cardiac tissue.[38] However, since mAChR antagonism abolished DMV light-induced bradycardias, this confirms that DMV neurons induce robust bradycardia through the canonical cardiovagal pathway nAChR→mAChR signaling (and not nAChR→nAChR).

DMV innervates cardiac tissue through the vagus nerve

Retrograde tracing with rhodamine and cholera toxin subunit B (CT-B) was done in male C57BL6/J mice to calculate the number of CVN^{DMV} and CVN^{NA} labeled by each tracer (n = 6–8 mice per tracer for each CVN group; Figures 2A and 2B). Although both tracers identified positive neurons in NA and DMV, there were fewer traced neurons in CVN^{DMV} (31 $\pm$ 19 neurons) compared to CVN^{NA} regardless of tracer (99 $\pm$ 16 neurons; repeated measure two-way ANOVA with Šídák's post hoc, p < 0.0001; Figure 2C). In all animals, both right and left DMV contained labeled cells regardless of tracer used. In one animal examined for right versus left distribution, the right DMV contained more retrograde labeling (68 neurons) compared to the left DMV (45 neurons). This pattern was similar to a previous report in rats.[39] In addition, CT-B (47 $\pm$ 36 neurons) labeled significantly fewer neurons than rhodamine regardless of region (83 $\pm$ 33 neurons; p = 0.0472). There was not a significant interaction between CVN location and tracer (p = 0.8294). To confirm that retrograde labeling of CVN^{DMV} required an intact vagus nerve, a unilateral left vagotomy prior to cardiac injection of rhodamine was performed in a separate group of animals (n = 3 mice, Figure 2D). Unilateral vagotomy eliminated labeling of CVN^{DMV} ipsilateral to vagotomy (2 $\pm$ 1 labeled CVN^{DMV}) compared to the contralateral side (32 $\pm$ 8 labeled CVN^{DMV}; two-tailed paired Student's *t* test, p = 0.0483; Figure 2E). Taken together, DMV contains neurons that retrogradely label from cardiac tissue in a vagus-dependent manner.

CVN^{DMV} show spontaneous firing and have larger input resistance *ex vivo* compared to CVN^{NA}

To characterize the electrophysiological properties of CVN^{DMV} in relation to CVN^{NA}, additional studies examined the general excitability of CVNs in male C57BL6/J mice using whole-cell patch-clamp electrophysiology under current clamp configuration. Retrogradely labeled CVNs were identified using visual inspection for rhodamine and anatomical landmarks (Figure 3A). Post hoc biocytin recovery confirmed location and cholinergic phenotype (Figure 3B). CVN^{DMV} exhibited more spontaneous firing (8/14 neurons from 10 mice) compared to CVN^{NA} (0/10 neurons from 9 mice; Mann Whitney test, p = 0.0064), which were completely devoid of any spontaneous firing activity (Figures 3C and 3D). Of CVN^{DMV} exhibiting spontaneous firing (57%), the average frequency was 1.28 $\pm$ 0.31 Hz.

No statistical differences in resting membrane potential were found between CVN^{DMV} (−58.60 $\pm$ 2.72 mV; n = 14 neurons from 10 mice) and CVN^{NA} (−62.18 $\pm$ 1.75 mV; n = 10 neurons from 9 mice; two-tailed unpaired Student's *t* test, p = 0.3256, Figure 3E). However, we found that CVN^{DMV} (492.00 $\pm$ 22.02 MΩ; n = 14 neurons from 10 mice) demonstrated significantly larger input resistance (R_{input}) than CVN^{NA}

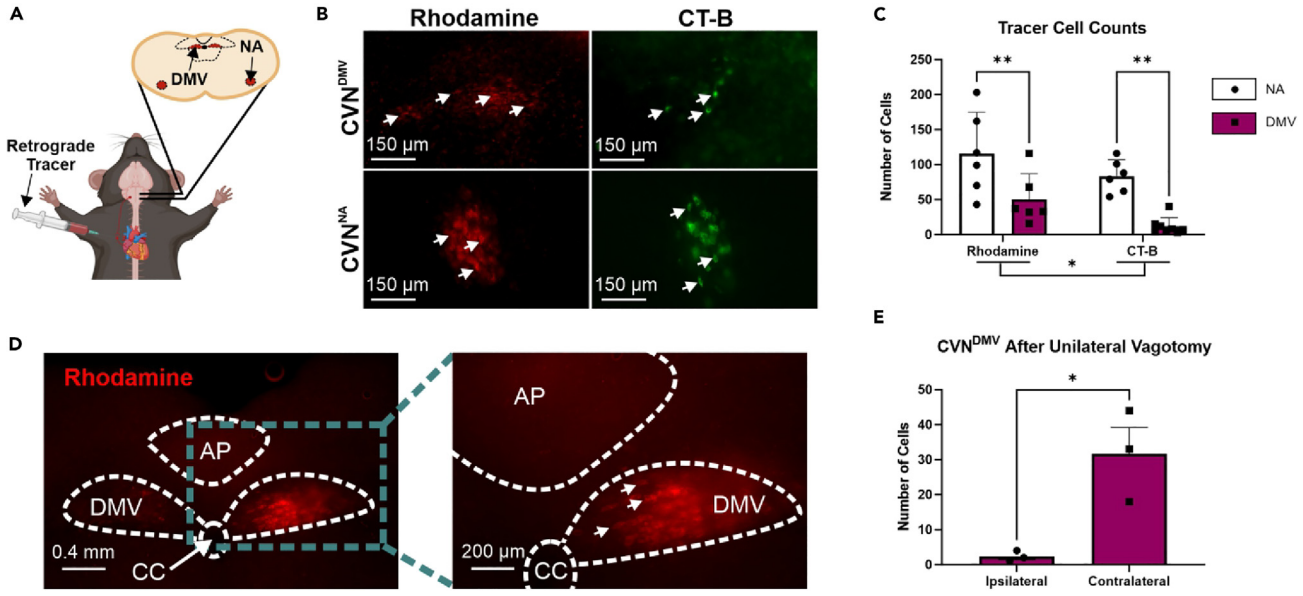

Figure 2. DMV innervates cardiac tissue through the vagus nerve in male mice

Schematic showing injection into the epicardial fat pad and labeling in both CVN brain regions (A). Representative images of DMV and NA after cardiac injection of retrograde tracers, rhodamine (left in red) and cholera toxin subunit B (CT-B; right in green) (B). Both rhodamine and CT-B significantly labeled cardiac projecting neurons in NA and DMV as analyzed by a repeated measure two-way ANOVA with Šídák's post hoc (C). Representative images of DMV after a right cervical vagotomy (C). Representative image (D) and mean cell count (E) showing a right cervical vagotomy significantly attenuated CVN^{DMV} numbers ipsilateral to vagotomy as analyzed by a two-tailed paired Student's *t* test. Bars represent mean and SEM. *p ≤ 0.05, **p ≤ 0.01, ***p ≤ 0.001, ****p ≤ 0.0001.

(158.20 ± 10.61 MΩ; n = 10 neurons from 9 mice; two-tailed unpaired Student's *t* test, p < 0.0001; Figures 3F–3H). Additionally, CVN^{DMV} (30.0 ± 1.5 pF) were significantly smaller in size than CVN^{NA} (61.1 ± 6.6 pF; two-tailed unpaired Student's *t* test, p < 0.0001) based on their recorded capacitance.

CVN^{DMV} are hyperexcitable compared to CVN^{NA} *ex vivo*

To determine if there were any differences in excitability between CVN^{DMV} and CVN^{NA}, CVNs were examined for general excitability through stepped depolarizations of current (Figure 3I). As expected, regardless of neuronal type, stepped current injections evoked a current dependent increase in action potential frequency (repeated measure two-way ANOVA with Šídák's post hoc, p < 0.0001; Figure 3J). Additionally, a significant effect of neuronal type regardless of current injection was found, with CVN^{DMV} exhibiting a significantly greater number of evoked action potentials (5 ± 1 number of action potentials, n = 14 neurons from 10 mice) compared to CVN^{NA} (2 ± 1 number of action potentials, n = 10 neurons from 9 mice; p < 0.0001). Finally, we found a significant interaction between current injection and neuronal type (p < 0.0001), with significantly more evoked action potentials in CVN^{DMV} compared to the CVN^{NA} at 100 (0.30 vs. 3.42 ± 0.5; p = 0.0001), 150 (0.80 vs. 5.00 ± 0.5; p < 0.0001), 200 (2.10 vs. 5.93 ± 0.5; p < 0.0001), and 250 pA (3.80 vs. 6.43 ± 0.6; p = 0.0017); Figure 3J). Taken together, CVN^{DMV} are more excitable than CVN^{NA}.

Chemogenetic activation of DMV suppresses HR for up to 8 h

Although our optogenetic studies could rule out interneuron activity, they could not exclude the possibility that off target stimulation of nearby Chat+ neurons (e.g., hypoglossal neurons) affected HR. Therefore, to confirm that activating DMV neurons decreases HR, we used an alternative strategy, chemogenetically activating DMV neurons with the excitatory designer receptor, hM3Dq. We specifically targeted hM3Dq expression to DMV neurons using an intersectional genetics approach which leverages the co-expression of *Chat* and *Phox2b* genes by DMV neurons but not by neighboring neurons (i.e., hypoglossal).[40,41] To validate this intersectional approach, $Chat^{Cre}$;$Phox2b^{Flp}$ mice were crossed with $R26^{ds-HTB}$ mice, a reporter line which expresses nuclear-localized, green fluorescent protein (GFP)-tagged histone 2b protein (H2b-GFP) upon recombination by both Cre and Flp. In the resulting $Chat^{Cre}$;$Phox2b^{Flp}$;$R26^{ds-HTB}$ mice, essentially all peripherally-projecting DMV neurons, as labeled by a systemic (*i.p.*) retrograde tracer, Fluoro-gold, were H2b-GFP immunofluorescent (136/139 DMV neurons from four mice (97.8%) were both Fluoro-gold+ and H2b-GFP+; representative image in Figure S1A). These results confirm that $Chat^{Cre}$ and $Phox2b^{Flp}$ are co-expressed by nearly all DMV vagal efferent neurons and thus validate our intersectional approach.

Next, to express hM3Dq specifically in DMV neurons, we injected an adeno-associated virus (AAV) which Cre- and Flp-dependently expresses a hemagglutinin (HA)-tagged hM3Dq (AAV1-CreON/FlpON-hM3Dq-HA; Figure 4A) into the DMV of male and female

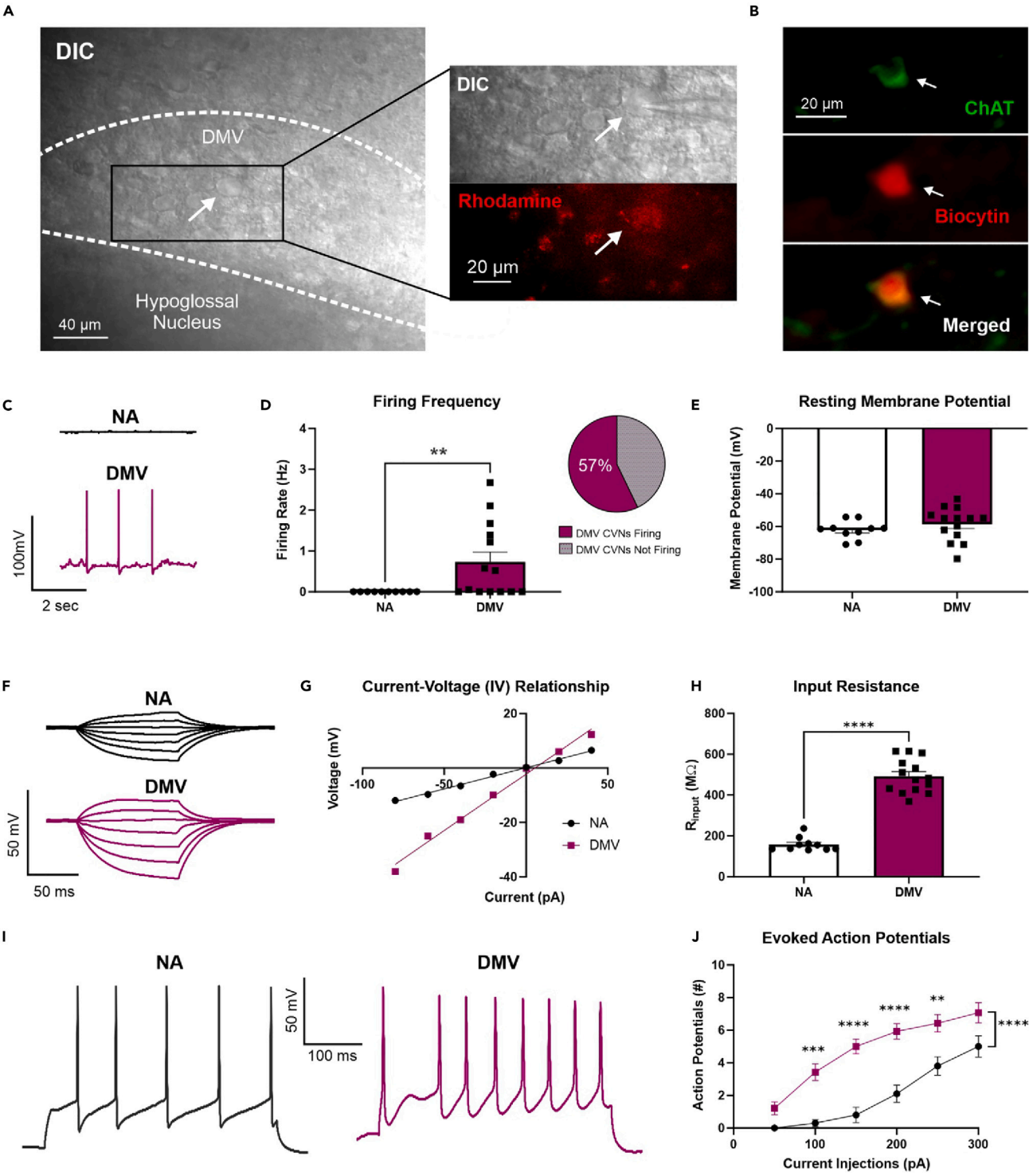

Figure 3. Differential electrophysiological properties of CVN^{DMV} compared to CVN^{NA} in male mice

Rhodamine-positive DMV neurons showing pipette (top) and rhodamine (bottom; red) (A). Representative immunofluorescence image of CVN^{DMV} showing biocytin recovered patched cardiac-labeled neurons are cholinergic (B). Representative trace (C) and mean firing rate (D) of CVN^{DMV} neurons show significantly higher spontaneous firing rates compared to CVN^{NA}, with the majority of CVN^{DMV} firing as analyzed by a Mann Whitney test. No statistical differences in resting membrane potential were found between CVN^{DMV} and CVN^{NA} using a two-tailed unpaired Student's *t* test (E). Representative traces of membrane responses from CVN^{NA} (top) and CVN^{DMV} (bottom) to stepped current injections (F). Current-voltage (I-V) relationship graph obtained from CVN^{NA} and CVN^{DMV} (G). R_{input} was higher in CVN^{DMV} compared to CVN^{NA} as analyzed by a two-tailed unpaired Student's *t* test (H). Representative action

Figure 3. *Continued*
potential responses in CVN^{NA} (top) and CVN^{DMV} (bottom) in response to 300 pA injection of direct depolarizing current (I). Action potential response curves were higher in CVN^{DMV} compared to CVN^{NA} in response to 50 pA-step injections of direct depolarizing current as analyzed by a repeated measure two-way ANOVA with Šídák's post hoc (J). Data represent mean and SEM. *p ≤ 0.05, **p ≤ 0.01, ***p ≤ 0.001, ****p ≤ 0.0001.

$Chat^{Cre}$;$Phox2b^{Flp}$;$R26^{ds-HTB}$ mice. This resulted in hM3Dq-HA expression in the vast majority of H2b-GFP+ DMV neurons ("DMV-hM3Dq" mice; Figures 4A–4C). Importantly, we failed to detect any hM3Dq-HA expression in NA of these mice (Figures 4B and 4C), or in DMV of mice lacking Cre and Flp recombinases (Figure S1B), confirming the specificity of our injection strategy and AAV expression.

To determine whether chemogenetically activating DMV neurons affects HR, we administered the hM3Dq ligand clozapine N-oxide (CNO; 1 mg/kg; *i.p.*) to DMV-hM3Dq mice while measuring HR by non-invasive electrocardiography (ECG; n = 8 mice per genotype). Administering CNO significantly decreased HR for up to 8 h compared to baseline (baseline: 718 ± 10 bpm; 20 min: 497 ± 34 bpm, p = 0.0012; 40 min: 497 ± 30 bpm, p = 0.0008; 60 min: 467 ± 36 bpm, p = 0.0007; 2h: 469 ± 39 bpm, p = 0.0011; 6h: 598 ± 19 bpm, p = 0.0006; 8h: 637 ± 24 bpm, p = 0.0274; Figure 4D). HR returned to baseline by 24 h post-CNO (24h: 731 ± 9 bpm, p = 0.7247). As expected, the acute bradycardia after CNO administration required peripheral muscarinic signaling, as it was abolished by administering the peripheral muscarinic blocker, methyl-atropine bromide (MA; 1.0 mg/kg; *i.p.*), 20min after CNO (baseline: 747 ± 5 bpm; after CNO: 640 ± 19 bpm vs. baseline, p = 0.0078; after MA: 801 ± 4 bpm vs. baseline, p = 0.0004; Figure 4E). On the other hand, administering CNO to hM3Dq-negative control mice failed to significantly alter HR (p > 0.05 vs. baseline or vehicle; Figures 4E and S1C), indicating that CNO alone did not affect HR. These results, together with our optogenetics studies, provide robust evidence that DMV neurons can decrease HR through peripheral muscarinic signaling.

Activating DMV neurons reduces anxiety-like behavior

Tachycardia increases anxiety-like behavior in mice,[29] consistent with the James-Lange theory that physiological cues can drive emotional states.[28] We therefore wondered whether the CNO-induced bradycardia in DMV-hM3Dq mice corresponded to any change in anxiety-like behavior. To investigate, male and female DMV-hM3Dq mice and control mice (n = 8 per group) were administered CNO or saline vehicle and then assessed behaviorally by the open field test, an assay which measures anxiety-like behavior based on time spent in the center of an open arena (Figure 4F).[42,43] Strikingly compared to vehicle, CNO treatment in DMV-hM3Dq mice significantly increased their time spent in the center of the open field (CNO: 85.31 ± 17.38 s vs. Vehicle: 64.55 ± 13.98 s; two tailed paired Student's *t* test, p = 0.0379, Figure 4G). The increased time spent in the center was not due to an increase in overall motility since total time spent moving did not differ significantly between saline and CNO treatments (two tailed paired Student's *t* test, p = 0.4643, Figure 4H). In addition, CNO's effects on HR and center time in DMV-hM3Dq mice were moderately correlated (R^2 = 0.7734, p = 0.0414; Figure 4I). Thus, activating DMV neurons caused a correlated decrease in HR and anxiety-like behavior in the open field test.

To confirm the change in anxiety-like behavior, we assessed another cohort of DMV-hM3Dq mice in a different measure of anxiety, the elevated plus maze[44] (Figure 4J). CNO treatment significantly increased the time DMV-hM3Dq mice spent in the open-arms of an elevated plus maze, relative to vehicle treatment, indicating a decrease in anxiety-like behavior (CNO: 16.9 ± 4.83 s vs. Vehicle: 0.23 ± 0.23 s, repeated measure ANOVA with Tukey's post hoc, p = 0.0235; Figure 4K). CNO treatment also significantly increased other signs of anxiolysis in DMV-hM3Dq mice: time spent moving (CNO: 162.6 ± 14.4 s vs. Saline: 40.7 ± 8.7 s; p = 0.0006; Figure 4L); head dip events (CNO: 4.149 ± 1.022 dips vs. Saline: 0.2414 ± 0.1424 dips; p = 0.0259; Figure S1E); and average velocity (CNO: 2.339 ± 0.3068 cm/s vs. Saline, 0.6606 ± 0.2317 s, p = 0.0011; Figure S1F). Importantly, however, treating hM3Dq-negative control mice with CNO did not affect their open-arm time, indicating that CNO itself does not decrease anxiety-like behavior (p = 0.3868; Figure S1D). In addition, co-administering MA ("CNO+MA") to DMV-hM3Dq mice largely prevented CNO's effects on measures of anxiolysis, indicating that DMV-induced anxiolysis, like DMV-induced bradycardia, required peripheral mAChR signaling (Figures 4K, S1E, and S1F). Specifically, compared to vehicle treatment, CNO+MA failed to significantly affect open-arm time, time spent moving, velocity or head dip events, relative to treatment with a saline vehicle (p < 0.05; Figures 4K, 4L, S1D, and S1E). The decrease in HR trended toward a moderate correlation with the increase in open-arm time (R^2 = 0.6394, p = 0.0878; Figure 4M). Thus, our results show that activating DMV neurons similarly decreases HR and anxiety-like behavior, and that these effects each depend on peripheral muscarinic signaling.

To identify the muscarinic receptors mediating anxiolysis, we repeated our HR and elevated plus maze studies on DMV-hM3Dq mice but used a selective inhibitor of muscarinic type 2 receptors (M2), AQ-RA 741 ("AQ"),[45] which does not appear to cross the blood-brain barrier.[46] Administering AQ after CNO reversed the CNO-induced bradycardia (repeated measure ANOVA with Tukey's post hoc, p = 0.0016; Figure S1G). Importantly, in contrast to CNO alone, administering CNO with AQ (CNO+AQ) did not significantly affect time spent in the open-arms relative to saline treatment (p = 0.2560; Figure 4N). These results suggest that activating DMV neurons decreases anxiety-like behavior through an M2-dependent mechanism.

DISCUSSION

The present study characterized CVN^{DMV} anatomically, physiologically, and functionally. Retrograde tracing from the cardiac fat pad confirmed the presence of CVN in DMV using two different tracers, rhodamine and CT-B, and this labeling required an intact vagus nerve. Electrophysiological comparison of retrogradely-labeled CVN^{DMV} and CVN^{NA} indicate distinct circuits, with CVN^{DMV} being significantly more excitable with higher input resistances and spontaneous activity *ex vivo* whereas CVN^{NA} were not. Optogenetically activating DMV neurons caused bradycardia, which was completely abolished by muscarinic and nicotinic antagonism. Finally, intersectional chemogenetic activation

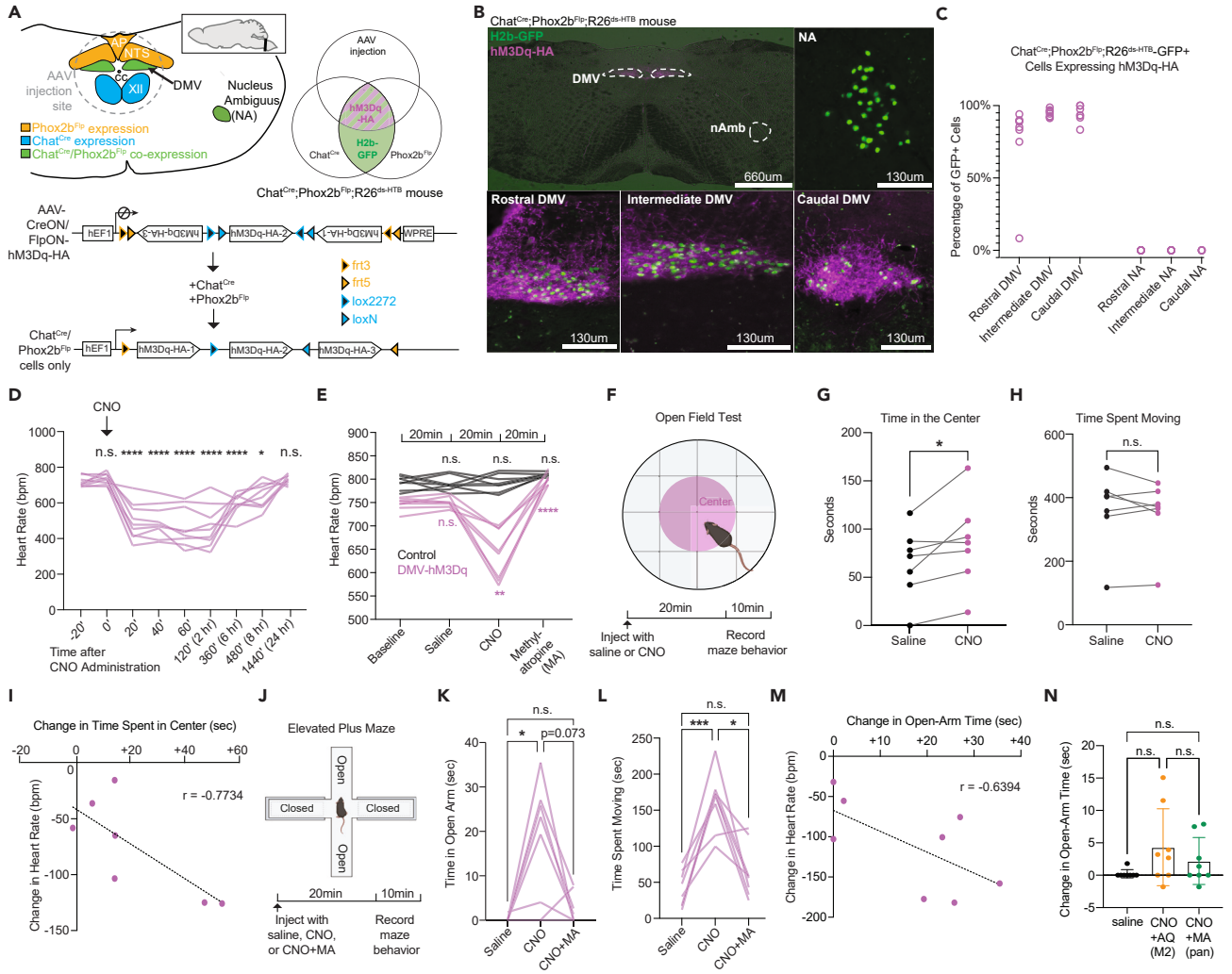

Figure 4. Chemogenetic stimulation of DMV produces bradycardia and reduces anxiety in both male and female mice

Illustration of coronal hindbrain section showing injection site and *Chat* and *Phox2b* expression (A, top left); Schematic of AAV1-CreON/FlpON-hM3Dq-HA viral construct (A, bottom); Venn diagram showing expected expression of hM3Dq-HA and H2b-GFP (A, top right). Representative images of rostral, intermediate, caudal DMV and NA stained for HA (magenta) and H2b-GFP (green) immunoreactivity in Chat^{Cre};Phox2b^{Flp};R26^{ds-HTB} mice after DMV injection of AAV1-CreON/FlpON-hM3Dq-HA (B). Percentage of H2b-GFP+ cells immunoreactive for hM3Dq-HA in the rostral, intermediate and caudal DMV and NA (C). Effect of CNO on HR in DMV-hM3Dq mice over 24-h period. CNO (1 mg/kg, *i.p.*) injected at time = 0 min. Data analyzed using repeated measure ANOVA with Tukey's post hoc (D). Effect of *i.p.* saline, CNO and CNO+MA on HR in DMV-hM3Dq (magenta) and control mice (black); comparisons are to baseline using a repeated measure ANOVA with Tukey's post hoc (E). Schematic of open field experiment (F). Effects of *i.p.* saline vehicle and CNO on time in the center (G) and time spent moving (H) for the open field, in seconds. Data analyzed using two tailed paired Student's *t* test (G,H). Correlation between changes in HR and center time between saline and CNO conditions in DMV-hM3Dq mice (I). Schematic of elevated plus maze (EPM) experiment (J). Effects of *i.p.* saline vehicle, CNO and CNO+MA administration on open-arm time (K) and time spent moving (L) in the elevated plus maze, in seconds. Data analyzed using repeated measure ANOVA with Tukey's post hoc (K, L). Pearson correlation between changes in HR and open-arm time between saline and CNO conditions in DMV-hM3Dq mice (M). Effects of *i.p.* MA and AQ-RA-741 on open-arm time in elevated plus maze, compared to saline; same saline and CNO+MA data as in Figure 4K. Data analyzed using repeated measure ANOVA with Tukey's post hoc (N). Data represent mean and SEM. *p ≤ 0.05, **p ≤ 0.01, ***p ≤ 0.001, ****p ≤ 0.0001.

of DMV neurons also caused bradycardia and a correlated decrease in anxiety-like behavior, both of which also required peripheral muscarinic signaling, as they were blocked by muscarinic antagonism.

Previous efforts to characterize *in vivo* electrophysiological properties of DMV neurons are limited, possibly a result of their prominent C-fiber phenotypes and long latency conduction times[33] making typical antidromic spike identification challenging. Our retrograde labeling findings are in accordance with previous reports, which suggest that only ~20% of CVN exist within DMV in totality (both sides), making the likelihood of recording from these numbers *in vivo* relatively low.[14] Importantly, CVNs signal organization is an established example of divergent amplification, meaning that changes in HR arise from modulation (activation or inhibition) of a relatively small number of CVNs.[30]

Therefore, whole-cell patch-clamp recordings paired with retrograde labeling in adult animals—albeit confounded by the absence of relevant synaptic inputs *in vivo*—is a powerful technique that future studies should continue to use to aid in the investigation of this population of neurons both in health and disease.

Our *ex vivo* results are consistent with electrophysiological recording in other DMV populations. DMV neurons demonstrate an on-going activity phenotype.[32,47,48] This was true in the present study as ~57% of CVN^{DMV} demonstrated a spontaneously active firing pattern during the recording period. With regards to CVNs, this on-going firing activity is unique to CVN^{DMV} since no CVN^{NA} recorded exhibited any spontaneous activity in our slice preparation, which is also consistent with previous results from CVN^{NA}.[31] While future studies will need to demonstrate how this spontaneous activity is generated, it is consistent with the intrinsic pace-making properties of other DMV neurons. However, it also suggests that CVN^{DMV} may represent a functionally discrete circuit for cardiac-related vagal motor output. Previous studies suggest that CVN^{DMV} have little respiratory-related burst activity, despite robust lung-related afferent activity,[33] which is in contrast to the CVN^{NA}, which show robust respiratory-related burst activity both *in vivo* and *ex vivo*.[9] While we are only beginning to elucidate the complexity of vagal circuits as it relates to any vagal motor output, there is increasing evidence for distinct circuits related to vagal sensory afferents. Similar distinct circuits also likely exist in vagal motor nuclei.[41,49,50] While some parallel circuits have converging anatomy and function, they may be distinct in terms of their physiological roles.[50] Finally, CVN^{DMV} demonstrated a significantly higher input resistance, higher number of spiking activity to current injections, and smaller size compared to CVN^{NA}. During optogenetic stimulation, CVN^{DMV} was also silenced for several seconds after stimulation implicating additional electrophysiological properties (i.e., unique ion channel contributions or stimulation-induced plasticity in neurotransmitter contributions) that could be investigated. Therefore, CVN^{DMV} are more excitable than CVN^{NA}. In other brain regions, this type of behavior confers a coincidence detection phenotype over a simple integrator.[51] Therefore, future work should continue to investigate how CVNs in NA and DMV differ in their microcircuit construction in relation to the basic circuit building blocks of critical homeostatic regulating networks.

Despite historical controversy about the capacity of CVN^{DMV} to impact HR, our results demonstrate that optogenetic and chemogenetic activation of Chat+ DMV neurons each caused robust bradycardia (~56% and ~65.5% of resting HR, respectively) in awake, behaving mice. Cardioinhibitory responses using optogenetic techniques in urethane-anesthetized rats and ketamine/xylazine-anesthetized mice demonstrated variable strength of the response,[18,21] implicating differences in anesthesia for differences in effect size. Alternatively, previous species used (namely cats and rats) may exhibit a lesser degree of DMV driven bradycardia than mice because of differences in vagal tonus. Since mice have a lower vagal tone than rats for example,[52–54] CVN^{DMV} activation in mice may recruit a larger number of CVN^{DMV} which were not previously active. Although it is possible that fast decay kinetics of $NpHR^{EYFP}$ in the Ai39 mouse line limited the ability to significantly inhibit DMV neurons,[36] the lack of an effect on HR of optogenetic inhibition of DMV in mice is similar to previous reports using inhibitory chemogenetic receptors.[17] Therefore, while the present study introduced a significant refinement of techniques using $Chat^{cre}$ mice to eliminate the impact of known interneurons within DMV, it may suggest that CVN^{DMV} activity is not necessary for vagal contributions to resting HR, similar to a previous report.[17]

While our Chat-targeted approach avoids influence of interneurons within DMV, the anatomical proximity of vagal axons from NA and the optical fiber in DMV[55] raises the possibility that DMV stimulation resulted in axonal stimulation of CVN^{NA} neurons. However, we failed to detect c-Fos expression in NA and DMV contralateral to the optical fiber, despite robust c-Fos immunoreactivity in the ipsilateral DMV. In addition, direct photostimulation of the vagus nerve in $Chat^{cre}$;ChR2 animals did not produce bradycardia. Finally, the more specifically targeted chemogenetic receptor hM3Dq expressed in DMV, but not other nearby cholinergic regions such as NA or hypoglossal neurons, caused a similar cardioinhibition to DMV stimulation in $Chat^{cre}$;ChR2. Taken together, these data provide robust evidence that solely activating DMV is sufficient for cardioinhibition (Figure 1D).

As expected, pharmacological testing confirmed that DMV stimulation-induced bradycardia requires mACh receptor activation in mice, since scopolamine (but not atenolol) and MA abolished optogenetically- and chemogenetically-induced bradycardia, respectively. Notably, while the traditional concept of vagal motor signaling to cardiac tissue requires nicotinic receptor-dependent communication between preganglionic and postganglionic parasympathetic neurons, some studies report that intracardiac ganglia harvested from SA node also show mACh receptor-dependent neurotransmitter and calcium mobilization.[56] Additional studies have attributed pharmacological differences in vagal fiber activation to C-fiber (presumably from DMV) versus B-fiber bradycardia (presumably from NA) since hexamethonium did not block the HR responses to non-myelinated fiber activation in these studies.[57] Still, it is important to note that the aforementioned studies did not comment on whether postganglionic neurons were isolated from cardiac nodal cells, nor did they directly address the effect of neurotransmitter release on the observed HR responses. Our findings are in accordance with the canonical signaling pathway between preganglionic and postganglionic parasympathetic neurons, as pre-treatment with the mACh receptor antagonist, scopolamine, completely abolished light-induced bradycardia in $ChAT^{cre}$;ChR2 mice.

Recent research suggests that HR can influence emotional states, supporting a theory of emotion separately proposed by the physiologist Carl Lange and psychologist William James over a century ago. As explained by James: "*My thesis […] is that the bodily changes follow directly the Perception of the exciting fact, and that our feeling of the same changes as they occur IS the emotion.*".[58] In other words, the James-Lange theory holds that HR does not increase because of anxiety; rather, the perception of HR increase is the anxiety. Consistent with this theory, a recent study in mice demonstrated that optogenetically increasing HR is sufficient to drive anxiety-like behaviors in the elevated plus maze.[29] Inversely, beta-blockers such as propranolol, which robustly decrease HR,[59] also reduce anxiety-like behaviors in mice.[60,61] Beta-blockers and other drugs which decrease HR have shown promise for treating anxiety and related disorders,[62] though the mechanism is not yet known. Studies of brain activity in humans and mice suggest the insular cortex may play a key role in sensing HR and other interoceptive cues[29,63–65] and so could couple the perception of HR to emotional state.

Importantly, however, while our study is the first to our knowledge to demonstrate a correlation between vagally-mediated bradycardia and anxiolysis, more research is needed to establish a causal relationship. Our results with the cardioselective M2 receptor antagonist AQ-RA 741,[45] which does not appear to cross the blood-brain barrier,[46] suggests a cardiogenic mechanism for the anxiolysis we observed when activating DMV neurons. For instance, one possibility is that DMV decreases anxiety-like behavior by decreasing HR. This would agree with recent studies showing that optogenetically increasing HR is anxiogenic,[29] whereas pharmacologically decreasing HR is anxiolytic.[66] Indeed, the M2 receptors blocked by AQ-RA 741 are enriched in the heart relative to other organs innervated by the DMV[45,67] and are necessary for vagally-mediated bradycardia.[68] However, M2 receptors are also present in the gastrointestinal tract where they interact with M3 receptors to modulate smooth muscle contraction.[69] Therefore, our results do not rule out the possibility that DMV decreases anxiety-like behavior through its projections to the gut.[69,70] Further research, e.g., targeting organ-specific DMV circuits, is needed to establish the mechanism by which DMV neurons can decrease anxiety. Whether other physiological functions of DMV, such as gut motility, glucose metabolism, and suppressing inflammation,[59] are involved remains unknown.

In summary, this study demonstrates the existence of CVN^{DMV} neurons and the DMV's ability to suppress HR and anxiety-like behavior. The cardioinhibitory and behavioral effects both require mACh receptor activity, and our results also suggest that nACh receptors are involved in the signaling between CVN^{DMV} and cardiac parasympathetic neurons, implicating canonical vagal pathways in DMV's facilitation of cardioinhibitory activity. CVN^{DMV} also has distinct electrophysiological properties, namely spontaneous firing activity and higher R_{input}, compared to CVN^{NA} *in slice*. Therefore, we further speculate that CVN^{DMV} represents a unique population of CVNs, distinct from the more thoroughly characterized CVN^{NA}. Further research is needed to identify the molecular profile of CVN^{DMV}, the mechanisms underlying their distinct electrophysiological properties, and their physiological role.

Limitations of the study

In this study, our use of transgenic mouse lines allowed for more targeted cell populations (namely Chat expressing) than previously used and demonstrated that DMV can elicit robust changes in HR in response to opto- or chemogenetic stimulation. Although our retrograde tracing results confirm DMV axonal projections to cardiac tissue, currently no transgenic mouse line is known to provide specificity to DMV neurons projecting solely to cardiac tissue. A discussion on the implications of DMV's regulation of gastrointestinal systems and anxiety has already been included. However, it is also possible that global DMV stimulation changed other physiological outputs, namely respiration or blood pressure. With advances in cell type markers in this region,[71] future studies should focus on defining more specific cell population targeting approaches that will allow for more precise circuit maps of DMV's role in physiological function. Although our electrophysiological studies provide important information regarding membrane properties and signaling *ex vivo*, they do not perfectly replicate the activity levels of these neurons *in vivo* with fully intact circuits. Despite challenges associated with recording cardiac-specific populations *in vivo*, future studies should include *in vivo* cellular recordings to further our understanding of differences between these neuronal populations.

STAR★METHODS

Detailed methods are provided in the online version of this paper and include the following:

- KEY RESOURCES TABLE
- RESOURCE AVAILABILITY
  - Lead contact
  - Materials availability
  - Data and code availability
- EXPERIMENTAL MODEL AND STUDY PARTICIPANT DETAILS
  - Mice
- METHOD DETAILS
  - Optogenetic activation and HR
  - Optogenetic stimulation of the vagus nerve
  - Retrograde tracing
  - Vagotomy
  - Electrophysiology
  - Chemogenetic activation
  - Non-invasive electrocardiography
  - Open field
  - Elevated plus maze
  - Immunohistochemistry
- QUANTIFICATION AND STATISTICAL ANALYSIS

SUPPLEMENTAL INFORMATION

Supplemental information can be found online at https://doi.org/10.1016/j.isci.2024.109137.

ACKNOWLEDGMENTS

We gratefully acknowledge Martyn Goulding (Salk Institute) for the $R26^{ds-HTB}$ mouse line. We also thank Hanns Ulrich Zeilhofer and Hendrik Wildner for the AAV1-ConFon-hM3Dq construct which was produced by the University of Zurich Viral Vector Facility Funding was provided by a Pathway to Stop Diabetes Initiator Award 1-18-INI-14 and, an NIH R01 HL153916 to J.N.C., an NIH R01 HL157366 to C.R.B. and an NIH T32 HL007446 for M.M.S.

AUTHOR CONTRIBUTIONS

M.M.S., N.J.C., L.S.K., M.J., S.B.G.A., J.N.C., and C.R.B. designed experiments. M.M.S, L.E., and S.F. performed optogenetic and cardiac tracing studies, including HR analysis, and all histology/immunofluorescence. L.E. and C.R.B. performed electrophysiological studies. A question from G.E.H. inspired the study of anxiety-like behavior. N.J.C., L.S.K., M.E.C., and P.C.M. performed chemogenetic study of HR and anxiety-like behavior. N.J.C. and L.S.K. performed histology and immunofluorescence experiments related to chemogenetic studies. M.M.S., N.J.C., J.N.C., L.E., and C.R.B. prepared figures. M.M.S., N.J.C., L.S.K., C.R.B., and J.N.C. wrote the manuscript with input from all authors.

DECLARATION OF INTERESTS

Authors declare no competing interest.

Received: September 22, 2023
Revised: December 16, 2023
Accepted: February 1, 2024
Published: February 6, 2024

REFERENCES

1. Corbett, E.K., Batten, T.F., Kaye, J.C., Deuchars, J., and McWilliam, P.N. (1999). Labelling of rat vagal preganglionic neurones by carbocyanine dye DiI applied to the heart. Neuroreport *10*, 1177–1181. https://doi.org/10.1097/00001756-199904260-00004.
2. Hsieh, J.H., Chen, R.F., Wu, J.J., Yen, C.T., and Chai, C.Y. (1998). Vagal innervation of the gastrointestinal tract arises from dorsal motor nucleus while that of the heart largely from nucleus ambiguus in the cat. J. Auton. Nerv. Syst. *70*, 38–50. https://doi.org/10.1016/s0165-1838(98)00027-7.
3. Izzo, P.N., Deuchars, J., and Spyer, K.M. (1993). Localization of cardiac vagal preganglionic motoneurones in the rat: immunocytochemical evidence of synaptic inputs containing 5-hydroxytryptamine. J. Comp. Neurol. *327*, 572–583. https://doi.org/10.1002/cne.903270408.
4. Massari, V.J., Johnson, T.A., and Gatti, P.J. (1995). Cardiotopic organization of the nucleus ambiguus? An anatomical and physiological analysis of neurons regulating atrioventricular conduction. Brain Res. *679*, 227–240. https://doi.org/10.1016/0006-8993(95)00227-h.
5. Standish, A., Enquist, L.W., and Schwaber, J.S. (1994). Innervation of the heart and its central medullary origin defined by viral tracing. Science *263*, 232–234. https://doi.org/10.1126/science.8284675.
6. Ter Horst, G.J., Hautvast, R.W., De Jongste, M.J., and Korf, J. (1996). Neuroanatomy of cardiac activity-regulating circuitry: a transneuronal retrograde viral labelling study in the rat. Eur. J. Neurosci. *8*, 2029–2041. https://doi.org/10.1111/j.1460-9568.1996.tb00723.x.
7. Geis, G.S., and Wurster, R.D. (1980). Cardiac responses during stimulation of the dorsal motor nucleus and nucleus ambiguus in the cat. Circ. Res. *46*, 606–611. https://doi.org/10.1161/01.res.46.5.606.
8. Gilbey, M.P., Jordan, D., Richter, D.W., and Spyer, K.M. (1984). Synaptic mechanisms involved in the inspiratory modulation of vagal cardio-inhibitory neurones in the cat. J. Physiol. *356*, 65–78. https://doi.org/10.1113/jphysiol.1984.sp015453.
9. McAllen, R.M., and Spyer, K.M. (1977). Bradycardia produced by iontophoretic activation of preganglionic vagal motoneurones [proceedings]. J. Physiol. *269*, 49P.
10. Cheng, Z., Powley, T.L., Schwaber, J.S., and Doyle, F.J., 3rd (1999). Projections of the dorsal motor nucleus of the vagus to cardiac ganglia of rat atria: an anterograde tracing study. J. Comp. Neurol. *410*, 320–341.
11. Ford, T.W., Bennett, J.A., Kidd, C., and McWilliam, P.N. (1990). Neurones in the dorsal motor vagal nucleus of the cat with non-myelinated axons projecting to the heart and lungs. Exp. Physiol. *75*, 459–473. https://doi.org/10.1113/expphysiol.1990.sp003423.
12. Jones, J.F., Wang, Y., and Jordan, D. (1995). Heart rate responses to selective stimulation of cardiac vagal C fibres in anaesthetized cats, rats and rabbits. J. Physiol. *489*, 203–214. https://doi.org/10.1113/jphysiol.1995.sp021042.
13. Nosaka, S., Yamamoto, T., and Yasunaga, K. (1979). Localization of vagal cardioinhibitory preganglionic neurons with rat brain stem. J. Comp. Neurol. *186*, 79–92. https://doi.org/10.1002/cne.901860106.
14. Taylor, E.W., Leite, C.A.C., Sartori, M.R., Wang, T., Abe, A.S., and Crossley, D.A., 2nd (2014). The phylogeny and ontogeny of autonomic control of the heart and cardiorespiratory interactions in vertebrates. J. Exp. Biol. *217*, 690–703. https://doi.org/10.1242/jeb.086199.
15. Taylor, E.W., Wang, T., and Leite, C.A.C. (2022). An overview of the phylogeny of cardiorespiratory control in vertebrates with some reflections on the 'Polyvagal Theory'. Biol. Psychol. *172*, 108382. https://doi.org/10.1016/j.biopsycho.2022.108382.
16. Laughton, W.B., and Powley, T.L. (1987). Localization of efferent function in the dorsal motor nucleus of the vagus. Am. J. Physiol. *252*, R13–R25. https://doi.org/10.1152/ajpregu.1987.252.1.R13.
17. Machhada, A., Marina, N., Korsak, A., Stuckey, D.J., Lythgoe, M.F., and Gourine, A.V. (2016). Origins of the vagal drive controlling left ventricular contractility. J. Physiol. *594*, 4017–4030. https://doi.org/10.1113/JP270984.
18. Machhada, A., Hosford, P.S., Dyson, A., Ackland, G.L., Mastitskaya, S., and Gourine, A.V. (2020). Optogenetic Stimulation of Vagal Efferent Activity Preserves Left Ventricular Function in Experimental Heart Failure. JACC. Basic Transl. Sci. *5*, 799–810. https://doi.org/10.1016/j.jacbts.2020.06.002.
19. Falvey, A., Palandira, S.P., Chavan, S.S., Brines, M., Tracey, K.J., and Pavlov, V.A. (2023). Electrical stimulation of the dorsal motor nucleus of the vagus regulates inflammation without affecting the heart rate. Preprint at bioRxiv. https://doi.org/10.1101/2023.05.17.541191.
20. Sporton, S.C., Shepheard, S.L., Jordan, D., and Ramage, A.G. (1991). Microinjections of 5-HT1A agonists into the dorsal motor vagal nucleus produce a bradycardia in the atenolol-pretreated anaesthetized rat. Br. J. Pharmacol. *104*, 466–470. https://doi.org/10.1111/j.1476-5381.1991.tb12452.x.
21. Thompson, D.A., Tsaava, T., Rishi, A., Nadella, S., Mishra, L., Tuveson, D.A., Pavlov, V.A., Brines, M., Tracey, K.J., and Chavan, S.S. (2023). Optogenetic stimulation of the brainstem dorsal motor nucleus ameliorates acute pancreatitis. Front. Immunol. *14*, 1166212. https://doi.org/10.3389/fimmu.2023.1166212.
22. Ottaviani, M.M., Vallone, F., Micera, S., and Recchia, F.A. (2022). Closed-Loop Vagus Nerve Stimulation for the Treatment of Cardiovascular Diseases: State of the Art and Future Directions. Front. Cardiovasc. Med. *9*, 866957. https://doi.org/10.3389/fcvm.2022.866957.

23. Shivaswamy, T., Souza, R.R., Engineer, C.T., and McIntyre, C.K. (2022). Vagus Nerve Stimulation as a Treatment for Fear and Anxiety in Individuals with Autism Spectrum Disorder. J. Psychiatr. Brain Sci. *7*, e220007. https://doi.org/10.20900/jpbs.20220007.
24. Groves, D.A., and Brown, V.J. (2005). Vagal nerve stimulation: a review of its applications and potential mechanisms that mediate its clinical effects. Neurosci. Biobehav. Rev. *29*, 493–500. https://doi.org/10.1016/j.neubiorev.2005.01.004.
25. Peña, D.F., Engineer, N.D., and McIntyre, C.K. (2013). Rapid remission of conditioned fear expression with extinction training paired with vagus nerve stimulation. Biol. Psychiatry *73*, 1071–1077. https://doi.org/10.1016/j.biopsych.2012.10.021.
26. Souza, R.R., Powers, M.B., Rennaker, R.L., McIntyre, C.K., Hays, S.A., and Kilgard, M.P. (2022). Timing of vagus nerve stimulation during fear extinction determines efficacy in a rat model of PTSD. Sci. Rep. *12*, 16526. https://doi.org/10.1038/s41598-022-20301-9.
27. George, M.S., Ward, H.E., Jr., Ninan, P.T., Pollack, M., Nahas, Z., Anderson, B., Kose, S., Howland, R.H., Goodman, W.K., and Ballenger, J.C. (2008). A pilot study of vagus nerve stimulation (VNS) for treatment-resistant anxiety disorders. Brain Stimul. *1*, 112–121. https://doi.org/10.1016/j.brs.2008.02.001.
28. Lange, C.G., and James, W. (1967). The Emotions (Hafner Pub. Co.).
29. Hsueh, B., Chen, R., Jo, Y., Tang, D., Raffiee, M., Kim, Y.S., Inoue, M., Randles, S., Ramakrishnan, C., Patel, S., et al. (2023). Cardiogenic control of affective behavioural state. Nature *615*, 292–299. https://doi.org/10.1038/s41586-023-05748-8.
30. McAllen, R.M., and Spyer, K.M. (1978). Two types of vagal preganglionic motoneurones projecting to the heart and lungs. J. Physiol. *282*, 353–364. https://doi.org/10.1113/jphysiol.1978.sp012468.
31. Mendelowitz, D. (1996). Firing properties of identified parasympathetic cardiac neurons in nucleus ambiguus. Am. J. Physiol. *271*, H2609–H2614. https://doi.org/10.1152/ajpheart.1996.271.6.H2609.
32. Browning, K.N., Renehan, W.E., and Travagli, R.A. (1999). Electrophysiological and morphological heterogeneity of rat dorsal vagal neurones which project to specific areas of the gastrointestinal tract. J. Physiol. *517*, 521–532. https://doi.org/10.1111/j.1469-7793.1999.0521t.x.
33. Jones, J.F., Wang, Y., and Jordan, D. (1998). Activity of C fibre cardiac vagal efferents in anaesthetized cats and rats. J. Physiol. *507*, 869–880. https://doi.org/10.1111/j.1469-7793.1998.869bs.x.
34. Cheng, Z., Zhang, H., Guo, S.Z., Wurster, R., and Gozal, D. (2004). Differential control over postganglionic neurons in rat cardiac ganglia by NA and DmnX neurons: anatomical evidence. Am. J. Physiol. Regul. Integr. Comp. Physiol. *286*, R625–R633. https://doi.org/10.1152/ajpregu.00143.2003.
35. Cauley, E., Wang, X., Dyavanapalli, J., Sun, K., Garrott, K., Kuzmiak-Glancy, S., Kay, M.W., and Mendelowitz, D. (2015). Neurotransmission to parasympathetic cardiac vagal neurons in the brain stem is altered with left ventricular hypertrophy-induced heart failure. Am. J. Physiol. Heart Circ. Physiol. *309*, H1281–H1287. https://doi.org/10.1152/ajpheart.00445.2015.
36. Madisen, L., Mao, T., Koch, H., Zhuo, J.M., Berenyi, A., Fujisawa, S., Hsu, Y.W.A., Garcia, A.J., 3rd, Gu, X., Zanella, S., et al. (2012). A toolbox of Cre-dependent optogenetic transgenic mice for light-induced activation and silencing. Nat. Neurosci. *15*, 793–802. https://doi.org/10.1038/nn.3078.
37. McGovern, A.E., and Mazzone, S.B. (2010). Characterization of the vagal motor neurons projecting to the Guinea pig airways and esophagus. Front. Neurol. *1*, 153. https://doi.org/10.3389/fneur.2010.00153.
38. Gee, M.M., Hornung, E., Gupta, S., Newton, A.J.H., Cheng, Z.J., Lytton, W.W., Lenhoff, A.M., Schwaber, J.S., and Vadigepalli, R. (2023). Unpacking the multimodal, multi-scale data of the fast and slow lanes of the cardiac vagus through computational modelling. Exp. Physiol. https://doi.org/10.1113/EP090865.
39. Takanaga, A., Hayakawa, T., Tanaka, K., Kawabata, K., Maeda, S., and Seki, M. (2003). Immunohistochemical characterization of cardiac vagal preganglionic neurons in the rat. Auton. Neurosci. *106*, 132–137. https://doi.org/10.1016/S1566-0702(03)00127-9.
40. Kang, B.J., Chang, D.A., Mackay, D.D., West, G.H., Moreira, T.S., Takakura, A.C., Gwilt, J.M., Guyenet, P.G., and Stornetta, R.L. (2007). Central nervous system distribution of the transcription factor Phox2b in the adult rat. J. Comp. Neurol. *503*, 627–641. https://doi.org/10.1002/cne.21409.
41. Tao, J., Campbell, J.N., Tsai, L.T., Wu, C., Liberles, S.D., and Lowell, B.B. (2021). Highly selective brain-to-gut communication via genetically defined vagus neurons. Neuron *109*, 2106–2115.e4. https://doi.org/10.1016/j.neuron.2021.05.004.
42. Christmas, A.J., and Maxwell, D.R. (1970). A comparison of the effects of some benzodiazepines and other drugs on aggressive and exploratory behaviour in mice and rats. Neuropharmacology *9*, 17–29. https://doi.org/10.1016/0028-3908(70)90044-4.
43. Crawley, J.N. (1985). Exploratory behavior models of anxiety in mice. Neurosci. Biobehav. Rev. *9*, 37–44. https://doi.org/10.1016/0149-7634(85)90030-2.
44. Lister, R.G. (1987). The use of a plus-maze to measure anxiety in the mouse. Psychopharmacology (Berl) *92*, 180–185. https://doi.org/10.1007/BF00177912.
45. Doods, H., Entzeroth, M., and Mayer, N. (1991). Cardioselectivity of AQ-RA 741, a novel tricyclic antimuscarinic drug. Eur. J. Pharmacol. *192*, 147–152. https://doi.org/10.1016/0014-2999(91)90081-z.
46. Cohen, V.I., Jin, B., Gitler, M.S., Delacruz, R.A., Boulay, S.F., Sood, V.K., Zeeberg, B.R., and Reba, R.C. (1995). Novel Potent and M(2)-Selective Antimuscarinic Compounds Which Penetrate the Blood-Brain-Barrier. Eur. J. Med. Chem. *30*, 61–69. https://doi.org/10.1016/0223-5234(96)88210-9.
47. Travagli, R.A., Gillis, R.A., Rossiter, C.D., and Vicini, S. (1991). Glutamate and GABA-mediated synaptic currents in neurons of the rat dorsal motor nucleus of the vagus. Am. J. Physiol. *260*, G531–G536. https://doi.org/10.1152/ajpgi.1991.260.3.G531.
48. Travagli, R.A., and Gillis, R.A. (1994). Hyperpolarization-activated currents, IH and IKIR, in rat dorsal motor nucleus of the vagus neurons *in vitro*. J. Neurophysiol. *71*, 1308–1317. https://doi.org/10.1152/jn.1994.71.4.1308.
49. Coverdell, T.C., Abraham-Fan, R.J., Wu, C., Abbott, S.B.G., and Campbell, J.N. (2022). Genetic encoding of an esophageal motor circuit. Cell Rep. *39*, 110962. https://doi.org/10.1016/j.celrep.2022.110962.
50. Veerakumar, A., Yung, A.R., Liu, Y., and Krasnow, M.A. (2022). Molecularly defined circuits for cardiovascular and cardiopulmonary control. Nature *606*, 739–746. https://doi.org/10.1038/s41586-022-04760-8.
51. König, P., Engel, A.K., and Singer, W. (1996). Integrator or coincidence detector? The role of the cortical neuron revisited. Trends Neurosci. *19*, 130–137. https://doi.org/10.1016/s0166-2236(96)80019-1.
52. Swoap, S.J., Overton, J.M., and Garber, G. (2004). Effect of ambient temperature on cardiovascular parameters in rats and mice: a comparative approach. Am. J. Physiol. Regul. Integr. Comp. Physiol. *287*, R391–R396. https://doi.org/10.1152/ajpregu.00731.2003.
53. Carnevali, L., and Sgoifo, A. (2014). Vagal modulation of resting heart rate in rats: the role of stress, psychosocial factors, and physical exercise. Front. Physiol. *5*, 118. https://doi.org/10.3389/fphys.2014.00118.
54. Marmerstein, J.T., McCallum, G.A., and Durand, D.M. (2021). Direct measurement of vagal tone in rats does not show correlation to HRV. Sci. Rep. *11*, 1210. https://doi.org/10.1038/s41598-020-79808-8.
55. Standish, A., Enquist, L.W., Escardo, J.A., and Schwaber, J.S. (1995). Central neuronal circuit innervating the rat heart defined by transneuronal transport of pseudorabies virus. J. Neurosci. *15*, 1998–2012. https://doi.org/10.1523/JNEUROSCI.15-03-01998.1995.
56. Beker, F., Weber, M., Fink, R.H.A., and Adams, D.J. (2003). Muscarinic and nicotinic ACh receptor activation differentially mobilize Ca2+ in rat intracardiac ganglion neurons. J. Neurophysiol. *90*, 1956–1964. https://doi.org/10.1152/jn.01079.2002.
57. Ford, T.W., and McWilliam, P.N. (1986). The effects of electrical stimulation of myelinated and non-myelinated vagal fibres on heart rate in the rabbit. J. Physiol. *380*, 341–347. https://doi.org/10.1113/jphysiol.1986.sp016289.
58. James, W. (1884). What is an emotion? Mind *9*, 188–205.
59. Black, J.W., Crowther, A.F., Shanks, R.G., Smith, L.H., and Dornhorst, A.C. (1964). A New Adrenergic Betareceptor Antagonist. Lancet *1*, 1080–1081. https://doi.org/10.1016/s0140-6736(64)91275-9.
60. Gorman, A.L., and Dunn, A.J. (1993). Beta-adrenergic receptors are involved in stress-related behavioral changes. Pharmacol. Biochem. Behav. *45*, 1–7. https://doi.org/10.1016/0091-3057(93)90078-8.
61. Wohleb, E.S., Hanke, M.L., Corona, A.W., Powell, N.D., Stiner, L.M., Bailey, M.T., Nelson, R.J., Godbout, J.P., and Sheridan, J.F. (2011). beta-Adrenergic receptor antagonism prevents anxiety-like behavior and microglial reactivity induced by repeated social defeat. J. Neurosci. *31*, 6277–6288. https://doi.org/10.1523/JNEUROSCI.0450-11.2011.
62. Repova, K., Aziriova, S., Krajcirovicova, K., and Simko, F. (2022). Cardiovascular therapeutics: A new potential for anxiety treatment? Med. Res. Rev. *42*, 1202–1245. https://doi.org/10.1002/med.21875.
63. Critchley, H.D., Wiens, S., Rotshtein, P., Ohman, A., and Dolan, R.J. (2004). Neural systems supporting interoceptive awareness.

Nat. Neurosci. *7*, 189–195. https://doi.org/10.1038/nn1176.

64. Khalsa, S.S., Rudrauf, D., Feinstein, J.S., and Tranel, D. (2009). The pathways of interoceptive awareness. Nat. Neurosci. *12*, 1494–1496. https://doi.org/10.1038/nn.2411.
65. Hassanpour, M.S., Simmons, W.K., Feinstein, J.S., Luo, Q., Lapidus, R.C., Bodurka, J., Paulus, M.P., and Khalsa, S.S. (2018). The Insular Cortex Dynamically Maps Changes in Cardiorespiratory Interoception. Neuropsychopharmacology *43*, 426–434. https://doi.org/10.1038/npp.2017.154.
66. Woodman, R., Student, J., Miller, C., and Lockette, W. (2023). Ivabradine-Induced Bradycardia is Accompanied by Reduced Stress-Related Anxiety. Am. J. Hypertens. *36*, 316–323. https://doi.org/10.1093/ajh/hpad019.
67. Saternos, H.C., Almarghalani, D.A., Gibson, H.M., Meqdad, M.A., Antypas, R.B., Lingireddy, A., and AbouAlaiwi, W.A. (2018). Distribution and function of the muscarinic receptor subtypes in the cardiovascular system. Physiol. Genomics *50*, 1–9. https://doi.org/10.1152/physiolgenomics.00062.2017.
68. Fisher, J.T., Vincent, S.G., Gomeza, J., Yamada, M., and Wess, J. (2004). Loss of vagally mediated bradycardia and bronchoconstriction in mice lacking M2 or M3 muscarinic acetylcholine receptors. FASEB J *18*, 711–713. https://doi.org/10.1096/fj.03-0648fje.
69. Ehlert, F.J., Ostrom, R.S., and Sawyer, G.W. (1997). Subtypes of the muscarinic receptor in smooth muscle. Life Sci. *61*, 1729–1740. https://doi.org/10.1016/s0024-3205(97)00433-5.
70. Jiang, Y., Greenwood-Van Meerveld, B., Johnson, A.C., and Travagli, R.A. (2019). Role of estrogen and stress on the brain-gut axis. Am. J. Physiol. Gastrointest. Liver Physiol. *317*, G203–G209. https://doi.org/10.1152/ajpgi.00144.2019.
71. Coverdell, T.C., Abbott, S.B.G., and Campbell, J.N. (2024). Molecular cell types as functional units of the efferent vagus nerve. Semin. Cell Dev. Biol. *156*, 210–218. https://doi.org/10.1016/j.semcdb.2023.07.007.
72. Bourane, S., Grossmann, K.S., Britz, O., Dalet, A., Del Barrio, M.G., Stam, F.J., Garcia-Campmany, L., Koch, S., and Goulding, M. (2015). Identification of a spinal circuit for light touch and fine motor control. Cell *160*, 503–515. https://doi.org/10.1016/j.cell.2015.01.011.
73. National Research Council (US) Committee for the Update of the Guide for the Care and Use of Laboratory Animals (2011). Guide for the Care and Use of Laboratory Animals. https://doi.org/10.17226/12910.
74. Strain, M.M., Espinoza, L., Fedorchak, S., Littlejohn, E.L., Andrade, M.A., Toney, G.M., and Boychuk, C.R. (2023). Early central cardiovagal dysfunction after high fat diet in a murine model. Sci. Rep. *13*, 6550. https://doi.org/10.1038/s41598-023-32492-w.
75. Littlejohn, E.L., Espinoza, L., Lopez, M.M., Smith, B.N., and Boychuk, C.R. (2019). GABA(A) receptor currents in the dorsal motor nucleus of the vagus in females: influence of ovarian cycle and 5alpha-reductase inhibition. J. Neurophysiol. *122*, 2130–2141. https://doi.org/10.1152/jn.00039.2019.
76. Daigle, T.L., Madisen, L., Hage, T.A., Valley, M.T., Knoblich, U., Larsen, R.S., Takeno, M.M., Huang, L., Gu, H., Larsen, R., et al. (2018). A Suite of Transgenic Driver and Reporter Mouse Lines with Enhanced Brain-Cell-Type Targeting and Functionality. Cell *174*, 465–480.e22. https://doi.org/10.1016/j.cell.2018.06.035.
77. Golden, S.A., Covington, H.E., Berton, O., and Russo, S.J. (2011). A standardized protocol for repeated social defeat stress in mice. Nat. Protoc. *6*, 1183–1191. https://doi.org/10.1038/nprot.2011.361.
78. La-Vu, M., Tobias, B.C., Schuette, P.J., and Adhikari, A. (2020). To Approach or Avoid: An Introductory Overview of the Study of Anxiety Using Rodent Assays. Front. Behav. Neurosci. *14*, 145. https://doi.org/10.3389/fnbeh.2020.00145.
79. Schneider, C.A., Rasband, W.S., and Eliceiri, K.W. (2012). NIH Image to ImageJ: 25 years of image analysis. Nat. Methods *9*, 671–675. https://doi.org/10.1038/nmeth.2089.

STAR★METHODS

KEY RESOURCES TABLE

REAGENT or RESOURCE	SOURCE	IDENTIFIER
Antibodies		
Texas Red Avidin D	Vector Laboratories	Cat# A-2206, RRID:AB_2336751
rabbit anti-cFos	Synaptic Systems	Cat# 226 003; RRID:AB_2231974
donkey-anti-rabbit Alexa Fluor 488	Thermo Fisher Scientific	Cat# A32790, RRID:AB_2762833
donkey-anti-goat Alexa Fluor 568	Thermo Fisher Scientific	Cat# A-11057, RRID:AB_2534104
chicken-anti-HA	Aves Labs	Cat# ET-HA100, RRID:AB_2313511
goat anti-ChAT	Sigma Aldrich	Cat# AB144P, RRID:AB_2079751
donkey-anti-chicken Alexa Fluor 647	Thermo Scientific	Cat# A78952, RRID:AB_2921074
Vectashield with DAPI	Vector Laboratories	Cat# H-1000, RRID:AB_2336789
Bacterial and virus strains		
AAV1-CreON/FlpON-hM3Dq-HA	Viral Vector Facility, University of Zurich	Cat# vhW34-1
Chemicals, peptides, and recombinant proteins		
Scopolamine methybromide	Sigma Aldrich	S8502
Atenolol	Sigma Aldrich	A7655
Hexamethonium	Sigma Aldrich	H2138
Clozapine N-oxide	Tocris Bioscience	#6329
Methyl-atropine bromide	Sigma Aldrich	2870-71-5
Cholera toxin subunit-b (recombinant), Alexa Fluor™ 555 Conjugate	Thermo Fisher Scientific	C34776
Tetramethylrhodamine-5-(and-6)-isothiocyanate conjugated with 5(6)-TRITC (Rhodamine)	Thermo Fisher Scientific	T490
Kynurenic acid	Sigma Aldrich	K3375
Biocytin	Sigma Aldrich	B4261
AQ-RA 741	Tocris Bioscience	catalog #2292
Experimental models: Organisms/strains		
Mouse: ChR2; Ai32(RCL-ChR2(H134R)/EYFP	JAX	#024109, RRID:IMSR_JAX:024109
Mouse: NpHR: Ai39(RCL-eNpHR3.0/EYFP	JAX	#014539, RRID:IMSR_JAX:014539
Mouse: ChAT$^{IRES\text{-}cre}$: B6.129S-Chat$^{tm1(cre)Lowl}$/MwarJ	JAX	#031661, RRID:IMSR_JAX:031661
Mouse: Chat-Cre: Chat$^{tm1(cre)Lowl}$	JAX	#028861, RRID:IMSR_JAX:028861
Mouse: Phox2b-Flp: Tg(Phox2b-flpo)3276Grds	JAX	#022407, RRID:IMSR_JAX:022407
Mouse: R26$^{ds\text{-}HTB}$	Martyn Goulding, Bourane et al.[72]	NA
Mouse: CaTCh: Gt(ROSA)26Sor$^{tm80.1(CAG\text{-}COP4*L132C/EYFP)Hze}$	JAX	#025109, RRID:IMSR_JAX:025109
Mouse: C57BL6/J	JAX	#000664, RRID:IMSR_JAX:000664
Software and algorithms		
Spike2 v9.0	CED	https://ced.co.uk
DSI talker	CED	https://ced.co.uk
EzCG software	Mouse Specifics Inc	https://mousespecifics.com
EthoVision	Noldus	https://www.noldus.com
Prism 9	GraphPad	https://www.graphpad.com
ImageJ	Schneider et al., 2012	https://imagej.net/ij/
CorelDraw	CorelDraw	www.coreldraw.com

(*Continued on next page*)

Continued

REAGENT or RESOURCE	SOURCE	IDENTIFIER
pClamp 10.2	Molecular devices	https://www.moleculardevices.com
Clampex 10.6	Molecular devices	https://www.moleculardevices.com
Revolve Pro software	Revolve Healthcare	https://revolve.healthcare/

RESOURCE AVAILABILITY

Lead contact

Further information and requests for resources and reagents should be directed to and will be fulfilled by the lead contact, Carie R. Boychuk (BoychukC@missouri.edu).

Materials availability

This study did not generate new unique reagents.

Data and code availability

- All data reported in this paper will be shared by the lead contact upon request.
- This study did not report original code.
- Any additional information required to reanalyze the data reported in this paper is available from the lead contact.

EXPERIMENTAL MODEL AND STUDY PARTICIPANT DETAILS

Mice

All animal procedures were approved by the Institutional Animal Care and Use Committee (IACUC) at the University of Texas Health San Antonio (UTHSA) or University of Virginia (UVA). Procedures were in accordance with the National Institutes of Health Guide for the Care and Use of Laboratory Animals.[73] All mice were maintained under standard conditions with access to food and water *ad libitum* on a 14:10 light cycle in a temperature regulated room (23.9 ± 1.7°C) at the University of Texas Health San Antonio (UTHSA) or a 12:12 light cycle in a temperature regulated room (20.6 ± 1.9°C) at the University of Virginia (UVA). Mice were randomly assigned to experimental groups and age-matched (9-52 weeks old). Animals were group housed unless stated otherwise. Sex is stated in the figure legends. All mice are maintained on a C57BL6/J background unless otherwise specified, and genotyping was performed according to guidelines from Jackson Laboratory or by Transnetyx. C57BL6/J adult mice (JAX #000664) were used for all experiments if not otherwise defined. Male and female mice were used in an inclusion design.

To generate a colony of transgenic mice with a constitutive knock-in of channelrhodopsin (ChR2) or halorhodopsin (NpHR^{EYFP}) in cholinergic neurons (Chat^{cre};ChR2 and Chat^{cre};NpHR, respectively), mice harboring a Cre-dependent cation channel channelrhodopsin (ChR2; Ai32(RCL-ChR2(H134R)/EYFP; JAX#024109) or halorhodopsin (NpHR^{EYFP}; Ai39(RCL-eNpHR3.0/EYFP; JAX#014539) were crossed with a ChAT$^{IRES\text{-}cre}$ ("Chat^{cre}") mouse lines (B6.129S-Chat$^{tm1(cre)Lowl}$/MwarJ; JAX#031661). This breeding strategy generates mice expressing ChR2 or NpHR^{EYFP} in Chat neurons ("Chat^{cre};ChR2" and "Chat^{cre};NpHR" mice, respectively; Figure 1A).

For chemogenetic studies, Chat^{Cre};Phox2b^{Flp};R26$^{ds\text{-}HTB}$ mice (13-52 weeks old; body weight, 25 ± 5g) were generated by first breeding Chat-Cre mice (Chat$^{tm1(cre)Lowl}$; JAX #028861) to Phox2b-Flp mice (Tg(Phox2b-flpo)3276Grds; JAX #022407), and then crossing the Chat^{Cre};Phox2b^{Flp} offspring to R26$^{ds\text{-}HTB}$ mice (gift of Martyn Goulding, Salk Institute for Biological Studies). The R26$^{ds\text{-}HTB}$ mouse line expresses a nuclear-localized, green fluorescent protein (GFP)-tagged histone 2b protein from the Rosa26 locus upon recombination by both Cre and Flp.

METHOD DETAILS

Optogenetic activation and HR

For brain region specific optogenetic stimulation, Chat^{cre};ChR2, Chat^{cre};NpHR, or control (Chat^{cre}) mice were implanted with an optical fiber over DMV or NA. First, mice were anesthetized with isoflurane to effect on a heating pad. Surgical sites were shaved and aseptically prepared with betadine and alcohol. Mice were first implanted with a HR telemetry (HRT) device (DSI, ETA-F10 implants, catalog # 270-0160-001).[74] Briefly, a vertical midline abdominal incision was made through the skin and peritoneal cavity. The telemetry device was placed in the peritoneal cavity with the leads tunneled to protrude from the peritoneal space. HR leads were then sutured in place in Lead II configuration and the peritoneal cavity closed with 4-0 silk suture. Wound clips were used to close the abdominal incision.

Following HRT implantation, mice were fixed in a stereotaxic frame (Kopf Instruments, Model 962) and an optical fiber cannula (Thorlabs, 0.50 NA, Ø200 μm Core Multimode Fiber, FP200URT) was inserted through a hole drilled through the skull just dorsal to the DMV (from bregma; anterior/posterior: -7.43 mm, medial/lateral: 0.25 mm, dorsal/ventral: -2.65 mm) or NA (anterior/posterior: -7.31 mm, medial/lateral: 1.25 mm, dorsal/ventral: -3.95 mm). Optical fibers were secured using dental cement (A-M Systems, catalog # 525000 and 526000) and skull

screws (Plastics One, 0-80- X 1/16). Subcutaneous administration of analgesics (buprenorphine 0.1 mg/kg and carprofen 10 mg/kg) were administered on the day of surgery and as needed for pain relief. Mice were monitored post-operatively for three days and allowed a week for recovery and acclimation to recording chambers.

During optogenetic stimulation trials, awake, behaving mice were temporarily singly housed with water available *ad libitum*. Photostimulation was performed using a diode-pumped solid state blue (for $Chat^{cre}$;ChR2; 470 nm, Opto Engine LLC, MDL-III-470-300mW) or green laser (for $Chat^{cre}$;NpHR; 532 nm; Opto EngineLLC, MGL-III-532-300mW). Optical matching gel (Zeiss, Immersol 518F) was applied at the ferrule junction to reduce light loss. Transmission efficiency of all implanted lasers was confirmed prior to implantation ($\geq$14 mW, 26.2 $\pm$ 6.8 mW) with a light meter (ThorLabs, PM100D). Phototrials consisted of 30 s of 20 Hz stimulation at 25mW pulsed laser output for DMV and 8mW for NA. All recordings occurred between 12:00 and 18:00 hour. Signals from HRT probes were acquired at a sampling frequency of 1 kHz using the DSITalker interface (Cambridge Electronic Design Limited) connected to the MX2 PhysioTel telemetry hardware (Data Sciences Inc.). HR was acquired 30 s before photostimulation and during a 30 s photostimulation period using Spike 2 (version 9) software (Cambridge Electronic Design Limited). All probe placements were confirmed postmortem (Figure 1C).

For assessment of autonomic contributions to optogenetic stimulation, scopolamine methylbromide (1 mg/kg, Sigma Aldrich, catalog # S8502), a muscarinic acetylcholine receptor antagonist; atenolol (10 mg/kg, Sigma Aldrich, catalog # A7655), a β1 adrenergic receptor antagonist; and autonomic ganglionic blocker hexamethonium (30 mg/kg, Sigma Aldrich, catalog # H2138), a nicotinic ACh receptor (nAChR) antagonist, were injected intraperitoneally (*i.p.*). A minimum of 15 minutes was allotted after drug injection before optogenetic stimulation.

Optogenetic stimulation of the vagus nerve

$Chat^{cre}$;ChR2 mice (10-20 weeks old; body weight, 31 $\pm$ 6g) were anesthetized with ketamine/xylazine (100 mg/kg; 10 mg/kg) and placed on a heating pad before the surgical site was shaved and aseptically prepared with betadine and alcohol. A five mm cervical incision was made at midline. Blunt dissection was used to isolate the right cervical vagus nerve from the carotid sheath. Mineral oil was applied to the exposed nerve to keep it moist. An optogenetic probe was placed one mm from the exposed vagus nerve. After a 15-minute acclimation period, the vagus nerve was stimulated for 20 s at 20 Hz at an intensity of 25 mW. A total of three simulations were done with a 5-minute inter-stimulation interval.

Retrograde tracing

Mice were anesthetized with ketamine/xylazine (100 mg/kg; 10 mg/kg) and ventilated (CWE SAR-830/AP with mouse attachment 12-01020) in the supine position on a heating pad (37°C). The surgical site was shaved and aseptically prepared with betadine and alcohol. A small (~5 mm) incision was made to access the thoracic cavity and the pericardial sac was incised. Cholera toxin subunit-b (recombinant) conjugated with Alexa Fluor 488 (CT-B; 0.1 % v/v, 100 mM, Invitrogen, catalog # C34776) or tetramethylrhodamine-5-(and-6)-isothiocyanate conjugated with 5(6)-TRITC (rhodamine; 100 mL, Invitrogen T490) was then injected into the pericardial fat pad near the posterior right atrioventricular junction where cardiovagal nerve endings terminate. Surgical incisions were closed with 4-0 silk suture. Mice were monitored post-operatively for 3-6 days and allowed a week for recovery before experiments. Subcutaneous administration of analgesics (buprenorphine 0.1 mg/kg and carprofen 10 mg/kg) were administered on the day of surgery and as needed for pain relief.

Vagotomy

A subset of mice were anesthetized with ketamine/xylazine (100 mg/kg; 10 mg/kg) and ventilated (CWE SAR-830/AP, with mouse attachment 12-01020) in the supine position on a heating pad (37°C). The surgical site was shaved and aseptically prepared with betadine and alcohol before a 5 mm cervical incision was made at midline. Blunt dissection was used to isolate the right cervical vagus nerve from the carotid sheath. A ~ 2 mm section was transected from the left cervical vagal nerve—sparing the aortic depressor nerve—to prevent regrowth/reattachment of the nerve. The superficial muscle and the cutaneous layer of the neck were sutured close with 4-0 silk suture. Mice then underwent retrograde tracing procedures as detailed above. Brains were harvested for immunohistochemistry procedures six days after retrograde tracing.

Electrophysiology

Mice (9-11 weeks old; 24.17 $\pm$ 0.86 g) were deeply anesthetized with isoflurane (3-4% in O_2) to effect (*i.e.*, lack of tail-pinch response) and decapitated while anesthetized. Brainstems were rapidly removed and immediately submerged in ice-cold (0–4°C) artificial cerebrospinal fluid (aCSF) equilibrated with carbogen gas (95% O_2, 5% CO_2). The aCSF composition (in mM) was: 124 NaCl, 3 KCl, 26 $NaHCO_3$, 1.4 NaH_2PO_4, 11 glucose, 1.3-2 $CaCl_2$, and 1.3 $MgCl_2$.[75] Osmolarity of all solutions was 290–305 mOSM; pH = 7.3–7.4. Brainstems were mounted and 300 μm coronal slices containing DMV and NA were cut using a vibratome (Leica Biosystems). Slices were transferred to a holding chamber and incubated in warmed (32–34°C) oxygenated aCSF containing 1mM kynurenic acid (kyn-aCSF) for 20 min. Slices were then transferred to an oxygenated holding chamber at room temperature where they were maintained before being placed in a recording chamber mounted on a fixed stage of an upright microscope (BX51WI; Olympus), where they were continuously superfused again with warmed (32–34°C), oxygenated aCSF (not containing kyn).

Whole-cell patch-clamp recordings under current clamp configuration were performed using infrared illumination and differential interference contrast optics (IR-DIC) under visual control. For recordings, glass pipettes (2–5 MΩ; King Precision Glass) were filled with a solution

containing the following (in mM): 130 K+-gluconate, 1 NaCl, 5 EGTA, 10 HEPES, 1 $MgCl_2$, 1 $CaCl_2$, and Mg-ATP, pH titrated to 7.33-7.39 with KOH. Biocytin (Sigma Aldrich, catalog # B4261) was added to the internal solution to identify patched neuron identity and location post-recording. Action potential (AP) frequency, resting membrane potential (RMP), and input resistance (R_{input}) were measured. RMP was corrected for liquid junction potential post hoc (−7 mV). R_{input} was measured by injecting 400 ms current pulse of -80 to +40 pA in 20 pA increments. To measure AP response to depolarizing current pulses (400 ms) of increasing amplitude (50 to 300 pA), background current was injected to maintain the membrane potential of patched neurons at approximately −60 mV to ensure a consistent starting voltage between current injection sweeps. Number of APs during each depolarizing current step were counted.

Recordings were discarded if series resistance was >25 MΩ or changed by >20% throughout the course of the experiment. Average series resistance was 9.64 ± 1.01 MΩ in the DMV and 11.71 ± 1.55 MΩ in the NA. Electrophysiological signals were acquired at 10 kHz and recorded using an Axoclamp 700B amplifier (Molecular Devices), low-pass filtered at 2 kHz, and stored to a computer using a Digidata 1440A digitizer and pClamp 10.2 software (Molecular Devices). For all electrophysiological experiments, data from only one cell per slice was included for data analysis. No more than three cells were used from one animal per region. A minimum of 8-10 min following establishment of whole-cell configuration was used to allow equilibration of the intracellular recording pipette contents. Two min of continuous recording of steady-state activity was analyzed offline with Clampex 10.6 (Molecular Devices).

Chemogenetic activation

Adult $Chat^{Cre}$;$Phox2b^{Flp}$;$R26^{ds\text{-}HTB}$ mice and $R26^{ds\text{-}HTB}$ only control mice were anesthetized with ketamine (80 mg/kg) and xylazine (10 mg/kg) then placed in a stereotaxic frame and on a servo-controlled heating pad to maintain a 37.0 ± 0.2°C body temperature (RightTemp Jr.; Kent Scientific). Surgical sites were shaved and cleaned with betadine and isopropyl alcohol and injected with Nocita (long-lasting bupivacaine, 5.3 mg/kg, subcutaneously) for pre-operative analgesia. The dorsal surface of the medulla was then exposed by gently retracting the overlaying neck muscles and incising the meninges. A NanoJect III (Drummond Scientific, catalog # 3-000-207) was used to inject 40nL of adeno-associated virus (AAV) Cre/Flp-dependently expressing hemagglutinin (HA)-tagged hM3Dq (ssAAV-1/2-hEF1a/hTLV1-Con/Fon(HA_hM3D(Gq))-WPRE-hGHp(A), Viral Vector Facility, University of Zurich and ETH Zurich, catalog # vhW34-1) at each of 8 injection sites (320nL total volume) to ensure infection throughout the DMV (from calamus scriptorius; anterior/posterior: ±0.3 mm, medial/lateral ±0.15 mm, dorsal/ventral: -0.25 and -0.5 mm). Injections were made at 25nL/sec and the injection pipette was left in place for 5 minutes to minimize viral spread up the pipette track. After the final injection, the retracted muscles were sutured together over the injection site using absorbable sutures, and the skin was closed with Vetbond surgical glue. Mice were provided with Meloxicam Sustained-Release (ZooPharm; 5mg/kg; IP) for post-operative analgesia, 1 mL of lactated Ringers solution in 5% dextrose to support hydration, and returned to the vivarium when ambulatory. These AAV-injected $Chat^{Cre}$;$Phox2b^{Flp}$;$R26^{ds\text{-}HTB}$ mice are referred to as "DMV-hM3Dq" mice. Mice were monitored post-operatively for five days and allowed to fully recover for three weeks before acclimation to experimental environments and procedures.

Non-invasive electrocardiography

For 24-hour HR monitoring, mice were placed individually in portable electrocardiography (ECG) towers (ECGenie, Mouse Specifics Inc.) according to the manufacturer's instructions. ECG data were analyzed with EzCG software (Mouse Specifics, Inc.). After a 30 minute acclimation period, baseline HR measurements (-20 min timepoint) were obtained by averaging at least three 10 sec epochs, which were manually reviewed to exclude those containing motion artifacts. Mice were then intraperitoneally injected with CNO (1.0mg/kg) at time 0. HR measurements from at least three 10 sec epochs were averaged per mouse per time point: 0 min; 20 min; 40 min; 60 min; 120 min; 6 hr; 8 hr; and 24 hr. Mice were kept in the towers from the -20 min time point until the 60 min time point, after which they were returned to their cages with access to food and water. For the 120 min, 6 hr, and 8 hr time points, mice were placed back into the towers for ECG recording and then returned to their cages. After the 8 hr time point, mice were returned to the vivarium. For the 24 hr time point, mice were re-acclimated for 30 min in the towers before collecting ECG data. Male and female mice were run on separate days.

For acute HR monitoring, mice were housed individually in ECGenie towers. As controls, we used CaTCh mice, a Cre/Flp reporter strain ($Gt(ROSA)26Sor^{tm80.1(CAG\text{-}COP4*L132C/EYFP)Hze}$, JAX#025109,[76]) on a (129S6/SvEvTac x C57BL/6NCrl) genetic background. Mice were acclimated to the towers for 30 min before recording baseline HR measurements. At 20 min intervals, mice were temporarily removed from the towers and administered each of the following injections (i.p) in the order listed, in equal volumes per mouse: saline vehicle, CNO (1.0 mg/kg, Tocris Bioscience, catalog # 6329) and either CNO plus MA (CNO+MA) (CNO, 1.0 mg/kg; MA, 1.0 mg/kg, Sigma Aldrich, catalog # 2870-71-5) or CNO plus AQ-RA 741 (CNO+AQ) (CNO, 1.0 mg/kg; AQ, 1.0 mg/kg, Tocris Bioscience, catalog # 2292). HR measurements were recorded 15 min after each injection and averaged as described above. Other than temporary removal for injections, mice remained in the ECG towers for the duration of the experiment (approximately 1.5 hr).

Open field

The open field (OF) maze is made of composite plastics and consists of a single circular arena 100 cm in diameter, enclosed by a wall 40 cm in height (Figure 4F). The maze arena consists of a center and outer ring, with the center ring extending to a radius of 29.4 cm, representing $^1/_4$ of the total area.[77,78] The maze occupies a dedicated procedural room which is kept at constant temperature (19.0°C) and illumination (100-120 lumens). Barriers are used so that the experimenter cannot be seen while the mouse is in the maze. All mice were acclimated to the experimenter and handling a minimum of 5 days prior to testing. Additionally, mice were acclimated to the behavioral room and maze for 3 training sessions prior to testing. DMV-hM3Dq mice (n=7) were randomly assigned to two groups and the order of the two treatments – saline vehicle

and CNO 1.0mg/kg - was randomized. The experimenter running the OF test was blinded to drug treatment until after all treatments were complete. Just prior to testing, mice were acclimated to the behavior room for 30 min. Each mouse received one *i.p.* injection, either saline vehicle or CNO, 20 min prior to testing and was then gently placed into the center of the open field test. Mice are allowed free exploration of the maze for 10 mins. Mouse movement was tracked over this 10 min period using a video camera and automated tracking software (EthoVision, Noldus). The time in the center and total time spent moving was calculated for the 10 min period using Noldus EthoVision software (Figures 4G and 4H). The maze was wiped clean with 70% ethanol spray before each use.

Elevated plus maze

The elevated plus maze (EPM) is made of plexiglass and consists of four arms (two open without walls and two closed with walls) (Figure 4J). The maze sits approximately 0.6 meters above the floor, on a columnar platform, and underneath a video camera. The maze occupies a dedicated procedural room (see open field above) which is kept at constant temperature (66°C) and illumination (100-120 lumens). Barriers are used so that the experimenter cannot be seen while the mouse is in the maze. All mice were acclimated to the experimenter and handling a minimum of 5 days prior to testing. Additionally, mice were acclimated to the behavioral room and maze for 3 training sessions prior to testing. DMV-hM3Dq mice (see above; n=8) and their controls (n=8) were randomly assigned to four groups and the order of these four treatments was randomized: saline vehicle, CNO 1.0mg/kg, CNO+MA (CNO, 1.0 mg/kg; MA, 1.0mg/kg) and CNO+AQ (CNO, 1.0mg/kg; AQ-RA 741, "AQ", 1.0mg/kg). The experimenter running the EPM test was blinded to treatment until after all treatments were complete. Just prior to testing, mice were acclimated to the behavior room for 30 min. Each mouse received one *i.p.* injection, either saline vehicle, CNO, CNO+MA, or CNO+AQ, 20 min prior to testing and was then gently placed into the closed arm of the maze. Mice are allowed free exploration of the maze for each 10 min session. Mouse movement was tracked over this 10 min period using a video camera and automated tracking software (EthoVision, Noldus). The time spent in open-arms, time spent moving, velocity and head dip events are each calculated for the 10 min period using Noldus EthoVision software. Mice underwent each treatment condition twice, and results were averaged between the two trials. Mice were allowed at least 24 hours recovery between testing days. The maze was wiped clean with 70% ethanol spray before each use.

Immunohistochemistry

At the termination of optogenetic experiments, mice were deeply anesthetized with isoflurane then transcardially perfused with 0.1 M phosphate buffered saline (PBS) followed by 4% paraformaldehyde (PFA). Brains were cryoprotected in 30% sucrose before being sectioned (40 μm) on a cryostat at -19°C (Leica Biosystems; CM 1860). Immunohistochemistry was performed on free floating sections for the immediate early gene product, cFos protein, as a marker of neuronal activation (rabbit anti-cFos, 1:1000, Synaptic Systems, catalog # 226 003), and ChAT (goat anti-ChAT, 1:250, Sigma Aldrich, catalog # AB144P) to identify ChAT-positive motor neurons in DMV and NA. The following secondary antibodies were used: donkey-anti-rabbit (Alexa Fluor 488, 1:200, Invitrogen, catalog # A32790) and donkey-anti-goat (Alexa Fluor 568, 1:200, Invitrogen, catalog # A-11057). Negative controls were run without primary antibody.

At the termination of electrophysiology experiments, brain slices were post-fixed with 4% PFA and then cryoprotected in 30% sucrose for at least two days before being sectioned (40 μm) on a cryostat at -19°C. Biocytin-filled neurons were processed via avidin, Texas Red staining (TX Red Avidin D; 1:400; Vector Laboratories, catalog # A-2206). Free floating sections were also immuno-labeled for ChAT (goat anti-ChAT, 1:250, Sigma Aldrich, catalog # AB144P) to detect ChAT-positive motor neurons as detailed above.

At the termination of chemogenetic HR and behavioral studies, mice were transcardially perfused as described above. Brains were then cryoprotected in 25% sucrose solution before being sectioned (35 μm) on a freezing microtome (SM2010R, Leica Biosystems). Next, brain sections were washed 3 times for 5 minutes each in phosphate buffered saline (PBS) on a shaker. After washing, brain sections were incubated in blocking solution (PBS with 0.1% Triton X, PBT, plus 2% donkey serum) overnight at 4°C. Next, immunohistochemistry was performed on free floating sections for hemagglutinin (HA; reporter for hM3Dq expression) (chicken-anti-HA 1:200, Aves Labs, catalog # ET-HA100) and ChAT (goat anti-ChAT, 1:250, Sigma Aldrich, catalog # AB144P) on brain sections representing the rostral, mid, and caudal DMV. Primary antibodies were diluted in blocking solution and added to brain sections for 2 hours at room temperature. A second wash cycle (3 rounds of 5 min) with PBS is performed before transferring the brain sections to secondary antibody solution. The following secondary antibodies were used: donkey-anti-chicken (Alexa Fluor 647, 1:2000, Thermo Scientific, catalog # A78952) and donkey-anti-goat (Alexa Fluor 568, 1:200, Invitrogen, catalog # A-11057). All secondaries were diluted in blocking solution and left to incubate overnight at room temperature. Following secondary incubation, brain sections underwent a third wash cycle (3 rounds of 5 min) in PBS before brain tissue was then mounted on glass slides, cover-slipped with a DAPI-containing mounting medium (Vectashield, Vector Labs, catalog # H-1000), and imaged on a fluorescence microscope (Revolve, Echo) using filters suitable for the appropriate fluorescent dyes and the following objectives: Olympus 2x Apochromat PLAN APO 2X objective, numerical aperture (NA) 0.08, working distance (WD), 6.2mm; Olympus 10x Fluorite U PLAN PHASE FLUORITE 10X objective, Ph1 Phase, NA 0.30, WD 10mm; Olympus 20x Apochromat U PLAN S-APO 20X objective, NA 0.75, WD 0.6mm. Images were processed using Revolve Pro software and Image J.[79]

QUANTIFICATION AND STATISTICAL ANALYSIS

Results are reported as mean ± standard error of the mean (S.E.M.). For *in vivo* experiments, 'n' is the number of animals. For *ex vivo* experiments, 'n' is reported as number of recorded cells and the number of animals. These values are stated when appropriate throughout the Results and Figure Legends. Graph creation and statistical analysis was conducted in GraphPad Prism 9 (GraphPad Software). Specific

statistical tests are noted in the Results. In general, two-tailed Student's t-test was conducted with parametric data containing two groups (paired or unpaired when appropriate). A Mann Whitney test was conducted with non-parametric data containing two groups. A one-way ANOVA followed by *Tukey's* multiple comparisons was used when there was one independent variable and more than two groups. A two-way ANOVA followed by *Šídák's* Multiple Comparison Test was used when there were two independent variables. Repeated-measures ANOVA was used when comparing multiple timepoints within subjects. The Geisser-Greenhouse correction was used if the sphericity assumption for ANOVA was not met. Simple linear regression was used to examine the relationship between two continuous variables. Pearson correlation was used to examine the strength of the relationship between two variables. Differences were considered statistically significant if $p \leq 0.05$. Graphs indicate individual mouse data or mean and SEM.